A&A 516, A70 (2010)
DOI: 10.1051/0004-6361/200913922

Astronomy & Astrophysics

Hyperfine structure measurements of neutral niobium with Fourier transform spectroscopy

S. Kröger[1], A. Er[2], I. K. Öztürk[2], G. Başar[2], A. Jarmola[3], R. Ferber[3], M. Tamanis[3], and L. Začs[3]

[1] Hochschule für Technik und Wirtschaft Berlin, Fachbereich 1, Wilhelminenhofstr. 75A, 12459 Berlin, Germany
e-mail: sophie.kroeger@htw-berlin.de
[2] Istanbul University, Faculty of Science, Physics Department, 34134 Vezneciler, Istanbul, Turkey
[3] Laser Centre, The University of Latvia, Rainis Boulevard 19, 1586 Riga, Latvia

Received 21 December 2009 / Accepted 10 March 2010

ABSTRACT

Aims. We report on experimental studies of hyperfine structure splitting of neutral niobium.
Methods. We used high-resolution Fourier transform spectroscopy to record a spectrum of niobium produced with a hollow cathode discharge lamp in the range of wavenumbers from 10 000 cm^{-1} to 30 000 cm^{-1}.
Results. The magnetic dipole hyperfine structure constants A were determined for the 109 levels of odd parity by analyzing the profiles of 224 spectral lines. The A values of 57 of these level are reported for the first time.

Key words. atomic data – methods: laboratory – techniques: spectroscopic – line: profiles

1. Introduction

The abundance patterns of neutron-capture elements in stellar atmospheres play an important role in constraining theoretical models of nucleosynthesis for elements heavier than iron. The recent commissioning of high-resolution spectrographs installed on large-aperture telescopes greatly increased the capacity of abundance analysis. In order to extract more information from high resolution stellar spectra, it is necessary to take into account nuclear effects, such as hyperfine structure and isotopic shifts. Therefore, new laboratory studies of hyperfine structure constants are needed to calculate accurate abundances.

Niobium (Nb), with atomic number 41, is the third member of the 4*d*-transition group elements and plays an important role in the investigation of the nucleosynthesis of heavy elements. Nb belongs to the few elements with only one stable isotope. The atomic spectrum of this stable isotope ^{93}Nb with nuclear spin $I = 9/2$ is characterized by a broad hyperfine structure caused by the large nuclear magnetic dipole moment.

The fine and hyperfine structure of atomic niobium has been the subject of several experimental and theoretical investigations (Başar et al. 2008; Kröger 2007; Kröger et al. 2007, 2004; Bouzed et al. 2003; Kröger & Bouzed 2003; Singh et al. 1992; Singh & Rao 1989; Fraenkel et al. 1988). All recent experimental work has been performed using laser spectroscopic methods, which are restricted in the wavelength range accessible to the cw-lasers currently in use. By means of a Fourier transform (FT) spectrometer the wavelength range could be extended significantly.

In the present work the spectrum of Nb was recorded in the wavelength range from 330 nm to 1000 nm with a high resolution (up to 0.02 cm^{-1}) Fourier transform spectrometer. These data enabled us to determine the magnetic dipole hyperfine structure constants A of 109 levels of odd parity, more than half of which had been unknown up to now.

It should be noted that laboratory studies for singly ionized niobium Nb II have been performed recently by FT spectroscopy by Nilsson & Ivarsson (2008), which resulted in new and improved transition probabilities and hyperfine structure data.

2. Experiment

A niobium spectrum was produced with a hollow cathode discharge lamp cooled with liquid nitrogen (for details see Messnarz & Guthöhrlein 2000). Briefly, the hollow cathode, made from copper, was 20 mm long and had a 5 mm bore, the surface of which was covered by a 0.125 mm pure (99.9%) niobium foil. The cathode was placed symmetrically between two hollow aluminium anodes; the distance between the cathode and the anodes was around 1.5 mm. The hollow cathode discharge was produced in an argon atmosphere at a pressure of around 1.7 mbar. The optimal discharge current, which corresponds to the maximum discharge intensity that can be achieved without a high risk of causing a short circuit, was found to be about 110 mA. The current from a high power DC power supply was stabilized with a series resistor.

The spectrum of niobium was recorded in the wavelength range from 10 000 cm^{-1} to 30 000 cm^{-1} (see Fig. 1) with a high resolution Bruker IFS 125HR Fourier transform spectrometer in the Laser Centre of the University of Latvia. The entrance aperture of the spectrometer was 0.8 mm, and the resolution was fixed to 0.02 cm^{-1}. Each spectrum was obtained from typically 40 scans. A quartz beam splitter and a Hamamatsu R928 photomultiplier were used to detect the spectra. The calibration of each spectrum was confirmed by using Ar lines presented in a hollow cathode discharge. The position of the lines could be

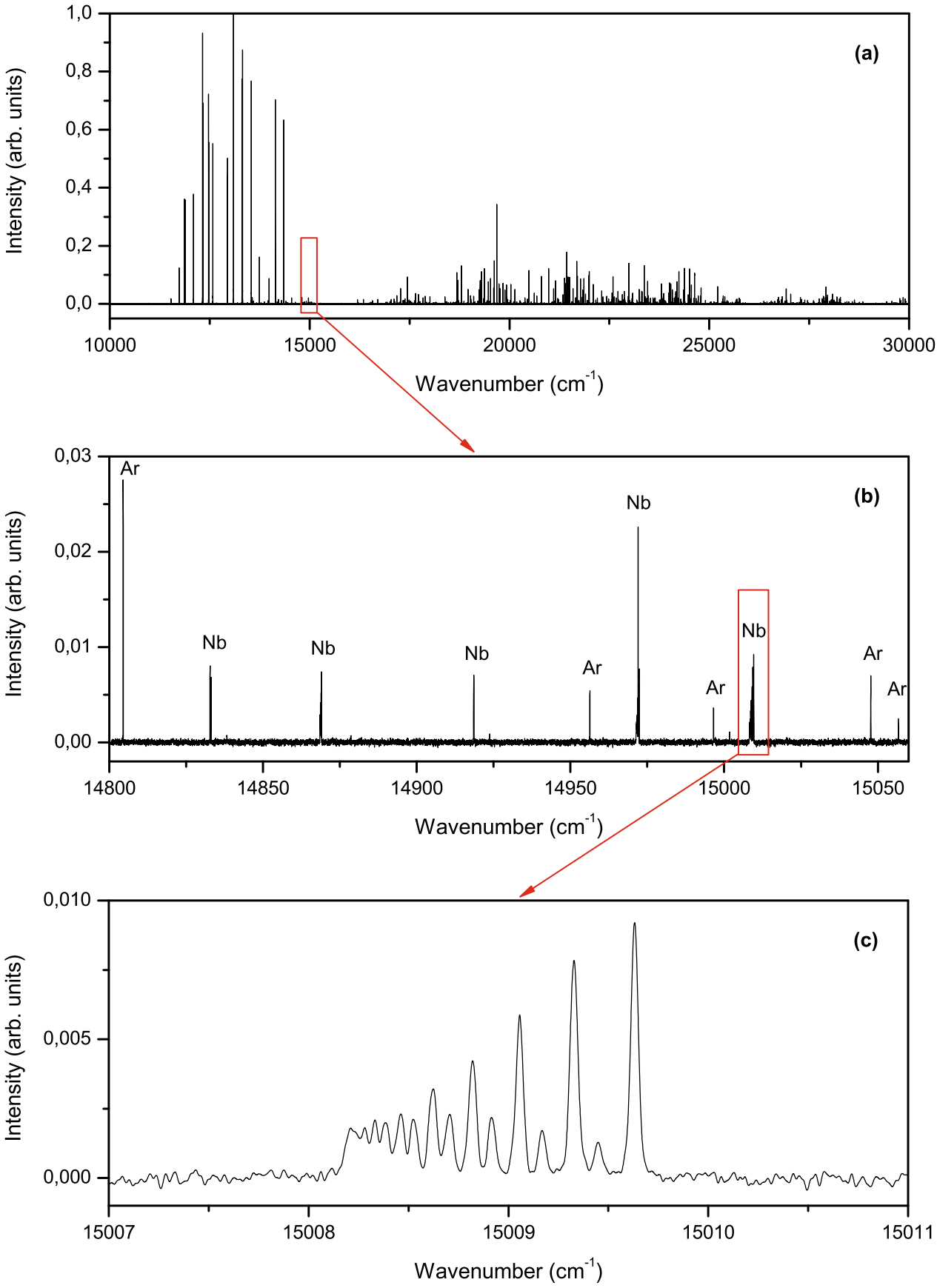

Fig. 1. Fourier transform spectrum of Nb I: **a)** full spectrum (the strong lines below 15 000 cm^{-1} belong to Ar), **b)** a part of the spectrum from 14 800 to 15 060 cm^{-1}, and **c)** enlarged view of the transition from the level 24 506.53 cm^{-1} (J = 9/2) to the level 9497.52 cm^{-1} (J = 7/2) at $\tilde{\nu}$ = 15 008.98 cm^{-1} or λ_{air} = 666.0840 nm, respectively.

determined with an accuracy better than 0.003 cm^{-1} for the entire wavelength range covered by the experiment.

Figure 1a presents an overview of the full spectrum from 10 000 cm^{-1} up to 30 000 cm^{-1}. Figure 1b shows a part of the spectrum as an example. Figure 1c zooms in further to show a single line.

The comprehensive list of experimental wavelengths of Nb from Humphreys & Meggers (1945)[1] helped us to identify the spectral lines of atomic Nb. All the lines, which are discussed in the next section, are listed in Table 1.

In the spectra a lot of Argon lines are visible as well, which are not the subject of interest of the present paper.

3. Hyperfine structure analysis

As mentioned above, the atomic spectrum of the stable isotope ^{93}Nb with nuclear spin $I = 9/2$ is characterized by a broad hyperfine structure caused by the large nuclear magnetic dipole moment $\mu_I = 6.1705\,(3)\ \mu_N$ (Lederer & Shirley 1978). Therefore, for most transitions it is reasonable to apply Doppler-limited, high-resolution experimental techniques like FT spectroscopy to accurately determine the hyperfine structure constants A. In contrast to the strong magnetic dipole interaction, the additional shift caused by the weak electric quadrupole interaction is very small for Nb, because the nuclear electric quadrupole moment $Q = -0.36\,(7)$ b (Lederer & Shirley 1978) is small. Thus, it was not possible to determine the electric quadrupole constants B for Nb from the FT spectra.

To investigate the hyperfine structure of a particular spectral line, the appropriate portion of the FT spectrum was cut out from the entire spectrum. Usually, the width of the structures ranged from 20 to 50 GHz.

The energy splitting of a fine structure level by the magnetic dipole hyperfine interactions is given by the well-known formula (see, for example, Cowan 1981)

$$W_F = \frac{1}{2} A\,[F(F+1) - J(J+1) - I(I+1)], \qquad (1)$$

where W_F is the energy of the hyperfine level with respect to the centre of gravity of the fine structure energy, while F, J, and I are the quantum numbers associated with the total angular momentum of the atom, the total angular momentum of the electrons, and the nuclear spin, respectively.

For the fitting procedure the program FITTER (Guthöhrlein 2004)[2] was utilized, which takes into account expression (1) for both levels involved in the transition. The program does an iterative least-squares fit to optimize the fit parameters, which in our case were the hyperfine structure constants A of the upper level and A_l and B_l of the lower level, the centre of gravity of the line, the peak intensity for each hyperfine component, and an appropriate line profile parameters. The fit program FITTER offers various line profile functions for the user to choose.

For the decision concerning the profile function and the fit parameter settings, fitting tests were done for lines with a completely resolved hyperfine structure. As a result of those tests, the Voigt profile function was chosen, which is a convolution of a Lorentzian profile and a Gaussian profile. The Voigt profile yields two profile parameters for the fit: the total full width at half maximum (FWHM), i.e., the Voigt FWHM, and the parameter θ, which lies between 0 and 1 and gives the ratio of the Gaussian to the Lorentzian part. From these two parameters, the Gaussian and the Lorentzian FWHM were calculated. The same profile parameters were used for all hyperfine components of a line.

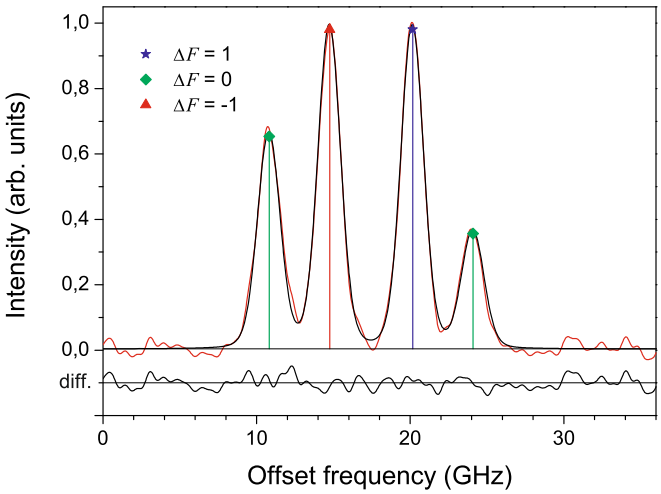

Fig. 2. Example of a resolved line: Fourier transform spectrum of the transition 20 107.36 cm^{-1} ($J = 1/2$) $\longrightarrow$ 0.00 cm^{-1} ($J = 1/2$) at λ_{air} = 497.1917 nm together with the best fitted curve. In the lower part of the figure, the residuals between the experiment and the fit are given. The components are assigned by the difference ΔF of the total angular momentum of the upper and lower hyperfine levels.

Additionally, the fitting tests demonstrated that the experimental intensities of the hyperfine components in the FT spectrum corresponded very well to the theoretical intensity ratios. Because most of lines were not completely resolved – some of them even were not resolved at all – the intensities of all hyperfine components were held at a constant ratio, which corresponded to the theoretical intensity ratio, during the fit.

As an example of a fit of a completely resolved hyperfine structure, the transition at λ_{air} = 497.1917 nm is shown in Fig. 2. In the lower part of the figure the residuals between the experiment and the fit are given. Only statistical noise can be seen, which suggests that the Voigt profile reproduces the experimental profile very well. Examples of a partially resolved line and of an unresolved line are presented in Figs. 3 and 4, respectively.

For all investigated transitions the lower level is the level of even parity, the A_l and B_l values of which are mostly very well known from high-resolution laser spectroscopic methods. The A_l and B_l values given in the literature are compiled in Table 2 for all levels of even parity that are involved in the transition under investigation. We decided to fix these values during the fit to increase the accuracy of the constants A of the odd parity upper levels, which were mostly unknown. The constants B of the upper levels were not taken into account for the reason mentioned above.

The whole spectrum was recorded eight times. For each line the mean value of the constant A that resulted from the fits of the eight measurements was determined. The measurement uncertainty for each value A was defined to be the corresponding standard deviation. In a few cases the measurement uncertainty of the hyperfine constant of the lower level, which was fixed during the fit, was higher than the standard deviation of the different fits. In these cases the measurement uncertainty of the hyperfine

[1] At the time, when the cited paper appeared, the element niobium was named columbium.

[2] The program FITTER (Guthöhrlein 2004) is also able to consider the electric quadrupole interaction in order to fit the B constants and to consider several different isotopes.

Table 1. Nb I transitions investigated by means of Fourier transform spectroscopy.

			Lower level		Upper level			
λ_{air}(nm)	$\tilde{\nu}$(cm^{-1})	Int.	E_l(cm^{-1})	J	E_u(cm^{-1})	J	$\tilde{\nu}_{fit}$(cm^{-1})	$\Delta\tilde{\nu}$(cm^{-1})
334.1982*	29 913.79	200 r	1142.79	3/2	31 056.60	5/2	29 913.84	–0.03
334.3712*	29 898.32	150 r	1586.90	5/2	31 485.20	7/2	29 898.32	–0.02
335.4743*	29 800.01	80	2805.36	9/2	32 605.39	9/2	29 800.03	0.00
338.0420*	29 573.66	40	1142.79	3/2	30 716.50	5/2	29 573.74	–0.03
353.7475	28 260.70	150	391.99	5/2	28 652.66	5/2	28 260.68	–0.01
355.4524*	28 125.16	60	2154.11	7/2	30 279.23	9/2	28 125.15	–0.03
355.4666*	28 124.03	80	154.19	3/2	28 278.25	3/2	28 124.08	–0.02
356.3501	28 054.31	100	154.19	3/2	28 208.48	3/2	28 054.30	–0.01
356.3624	28 053.34	80	391.99	5/2	28 445.33	5/2	28 053.36	–0.02
357.5850	27 957.43	200	695.25	7/2	28 652.66	5/2	27 957.43	–0.02
358.0277*	27 922.86	400 r	1050.26	9/2	28 973.12	7/2	27 922.87	–0.01
358.4972	27 886.29	100	391.99	5/2	28 278.25	3/2	27 886.28	–0.02
358.9106	27 854.17	100	695.25	7/2	28 549.42	5/2	27 854.18	–0.01
358.9356	27 852.23	100 c	2805.36	9/2	30 657.60	11/2	27 852.22	0.02
359.3966*	27 816.51	80	391.99	5/2	28 208.48	3/2	27 816.50	–0.01
360.2561	27 750.14	60	695.25	7/2	28 445.33	5/2	27 750.11	–0.03
362.1030*	27 608.61	40	2154.11	7/2	29 762.70	7/2	27 608.62	–0.03
364.9854	27 390.58	60	391.99	5/2	27 782.57	3/2	27 390.59	–0.01
366.0364	27 311.94	100	2805.36	9/2	30 117.32	9/2	27 311.94	0.02
366.4692*	27 279.68	80	695.25	7/2	27 974.87	9/2	27 279.68	–0.06
371.1343	26 936.79	60	0.00	1/2	26 936.86	3/2	26 936.84	0.02
371.3018	26 924.64	300 r	1050.26	9/2	27 974.87	9/2	26 924.65	–0.04
372.6235	26 829.14	250	154.19	3/2	26 983.34	5/2	26 829.15	0.00
373.9800	26 731.83	300 r	695.25	7/2	27 427.07	7/2	26 731.85	–0.03
374.1776*	26 717.71	30 c	0.00	1/2	26 717.73	1/2	26 717.72	0.01
374.2393	26 713.31	200 r	0.00	1/2	26 713.32	3/2	26 713.31	0.01
376.3492	26 563.55	40	154.19	3/2	26 717.73	1/2	26 563.54	0.00
387.8817	25 773.78	40	391.99	5/2	26 165.79	7/2	25 773.78	0.02
388.3141	25 745.08	80	695.25	7/2	26 440.33	9/2	25 745.09	–0.01
389.1302	25 691.09	60	695.25	7/2	26 386.36	5/2	25 691.14	–0.03
389.3733	25 675.05	40	391.99	5/2	26 067.06	3/2	25 675.07	0.00
389.4039	25 673.03	50	11 044.08	9/2	36 717.11	9/2	25 673.05	–0.02
390.8971	25 574.96	40	1142.79	3/2	26 717.73	1/2	25 574.94	0.00
393.7437	25 390.07	150	1050.26	9/2	26 440.33	9/2	25 390.06	0.01
394.3663	25 349.99	60	1586.90	5/2	26 936.86	3/2	25 349.97	–0.01
396.5692	25 209.17	40	5965.45	5/2	31 174.65	3/2	25 209.18	0.02
396.6246	25 205.65	150	2154.11	7/2	27 359.70	5/2	25 205.61	–0.02
398.0483*	25 115.50	60 c	1050.26	9/2	26 165.79	7/2	25 115.49	0.04
403.2524	24 791.39	150	2805.36	9/2	27 596.74	7/2	24 791.38	0.00
403.3195	24 787.26	40	1142.79	3/2	25 930.01	3/2	24 787.23	–0.01
405.1513*	24 675.19	25	9328.88	9/2	34 004.08	11/2	24 675.20	0.00
405.8933*	24 630.08	2000 c	1050.26	9/2	25 680.36	11/2	24 630.09	0.01
405.9498	24 626.66	40	10 126.06	1/2	34 752.70	3/2	24 626.64	0.00
406.0800	24 618.76	40 c	154.19	3/2	24 773.03	5/2	24 618.84	0.00
407.9726*	24 504.56	1000 c	695.25	7/2	25 199.81	9/2	24 504.55	0.01
408.4861	24 473.75	40	1586.90	5/2	26 060.65	5/2	24 473.75	0.00
409.9067	24 388.93	30	154.19	3/2	24 543.13	5/2	24 388.92	0.02
410.0389	24 381.07	80	391.99	5/2	24 773.03	5/2	24 381.04	0.00
410.0918	24 377.93	600 c	391.99	5/2	24 769.91	7/2	24 377.91	0.01
411.3941*	24 300.76	25	11 044.08	9/2	35 344.86	11/2	24 300.75	0.03
411.6895	24 283.32	50	0.00	1/2	24 283.34	3/2	24 283.30	0.04
412.3812	24 242.59	400	154.19	3/2	24 396.80	5/2	24 242.60	0.01
412.9430	24 209.61	100 c	695.25	7/2	24 904.86	7/2	24 209.62	–0.01
412.9931	24 206.67	150 c	11 524.65	13/2	35 731.34	15/2	24 206.68	0.01
413.7090*	24 164.79	200	0.00	1/2	24 164.79	3/2	24 164.77	0.02
413.9430	24 151.13	90 c	391.99	5/2	24 543.13	5/2	24 151.12	0.02
413.9702	24 149.54	400 c	1050.26	9/2	25 199.81	9/2	24 149.52	0.03
414.3201	24 129.15	80 c	154.19	3/2	24 283.34	3/2	24 129.12	0.03
415.2040	24 077.78	20 c	695.25	7/2	24 773.03	5/2	24 077.79	–0.01
415.2575	24 074.68	500	695.25	7/2	24 769.91	7/2	24 074.65	0.01
416.3474	24 011.66	40	2154.11	7/2	26 165.79	7/2	24 011.65	0.03
416.3658	24 010.60	250	154.19	3/2	24 164.79	3/2	24 010.59	0.01
416.4661	24 004.81	300	391.99	5/2	24 396.80	5/2	24 004.80	0.01
416.8122	23 984.88	250 c	0.00	1/2	23 984.87	1/2	23 984.85	0.02

Table 1. continued.

			Lower level		Upper level			
λ_{air}(nm)	$\tilde{\nu}$(cm^{-1})	Int.	E_l(cm^{-1})	J	E_u(cm^{-1})	J	$\tilde{\nu}_{fit}$(cm^{-1})	$\Delta\tilde{\nu}$(cm^{-1})
418.4440	23 891.35	50 c	391.99	5/2	24 283.34	3/2	23 891.32	0.03
419.0889	23 854.59	150 c	1050.26	9/2	24 904.86	7/2	23 854.58	0.02
419.2065	23 847.90	100 c	695.25	7/2	24 543.13	5/2	23 847.87	0.01
419.5096	23 830.66	80	154.19	3/2	23 984.87	1/2	23 830.68	0.00
419.8510	23 811.29	30	695.25	7/2	24 506.53	9/2	23 811.29	–0.01
420.1519	23 794.24	40	11 044.08	9/2	34 838.33	11/2	23 794.24	0.01
420.5308	23 772.80	120	391.99	5/2	24 164.79	3/2	23 772.79	0.01
420.8156	23 756.71	30	154.19	3/2	23 910.90	1/2	23 756.69	0.02
421.4732	23 719.64	100 c	1 050.26	9/2	24 769.91	7/2	23 719.62	0.03
421.7946	23 701.57	150 c	695.25	7/2	24 396.80	5/2	23 701.54	0.01
422.9154	23 638.76	100 c	9497.52	7/2	33 136.30	9/2	23 638.77	0.01
422.9832	23 634.97	25	2805.36	9/2	26 440.33	9/2	23 634.96	0.01
423.1954	23 623.14	25	391.99	5/2	24 015.11	7/2	23 623.11	0.01
424.9457	23 525.82	20	0.00	1/2	23 525.80	3/2	23 525.80	0.00
425.4693	23 496.87	30	8410.90	1/2	31 907.74	3/2	23 496.85	–0.01
425.5439	23 492.75	60 c	10 922.74	7/2	34 415.52	9/2	23 492.74	0.04
426.2056	23 456.28	100	1050.26	9/2	24 506.53	9/2	23 456.26	0.01
426.6020	23 434.48	50	8705.32	3/2	32 139.78	5/2	23 434.47	–0.01
426.8667	23 419.95	15	154.19	3/2	23 574.14	5/2	23 419.94	0.01
427.0691	23 408.85	50 c	9043.14	5/2	32 451.99	7/2	23 408.85	0.00
427.7500*	23 371.59	20	11 044.08	9/2	34 415.52	9/2	23 371.41	0.03
428.6987	23 319.87	60	695.25	7/2	24 015.11	7/2	23 319.85	0.01
428.9443	23 306.52	30	5965.45	5/2	29 271.99	7/2	23 306.51	0.03
429.1195*	23 297.00	25	8410.90	1/2	31 707.94	3/2	23 297.02	0.02
429.2035	23 292.44	20 c	391.99	5/2	23 684.44	5/2	23 292.44	0.01
429.2480	23 290.03	40 c	9043.14	5/2	32 333.18	7/2	23 290.05	–0.01
429.9596	23 251.48	100	5297.92	3/2	28 549.42	5/2	23 251.49	0.01
430.0989	23 243.95	100	5965.45	5/2	29 209.42	7/2	23 243.95	0.02
430.6283*	23 215.38	15	9439.08	3/2	32 654.48	5/2	23 215.39	0.01
431.2454	23 182.15	25	391.99	5/2	23 574.14	5/2	23 182.15	0.00
432.6320	23 107.86	100 c	9497.52	7/2	32 605.39	9/2	23 107.85	0.02
432.9732	23 089.65	20 c	154.19	3/2	23 243.87	3/2	23 089.64	0.04
433.1371	23 080.91	60	4998.17	1/2	28 079.09	3/2	23 080.91	0.01
434.2818	23 020.07	25	12 136.86	7/2	35 156.94	9/2	23 020.08	0.00
434.5315	23 006.84	20 d	0.00	1/2	23 006.86	3/2	23 006.82	0.04
434.8652	22 989.19	40	695.25	7/2	23 684.44	5/2	22 989.18	0.01
435.1573	22 973.76	40	8827.00	7/2	31 800.74	7/2	22 973.75	–0.01
435.3266	22 964.83	20	1050.26	9/2	24 015.11	7/2	22 964.82	0.03
436.8434	22 885.09	50	9328.88	9/2	32 213.94	9/2	22 885.07	–0.01
438.7743	22 784.38	15	4998.17	1/2	27 782.57	3/2	22 784.37	0.03
438.8357	22 781.19	30	5297.92	3/2	28 079.09	3/2	22 781.18	–0.01
439.2692*	22 758.71	30	9328.88	9/2	32 087.58	7/2	22 758.69	0.01
441.0214	22 668.29	60	4998.17	1/2	27 666.46	1/2	22 668.29	0.00
441.1526	22 661.55	15	10 237.51	5/2	32 899.08	7/2	22 661.56	0.01
441.9448	22 620.93	40	5297.92	3/2	27 918.85	3/2	22 620.92	0.01
442.0637	22 614.84	30 c	391.99	5/2	23 006.86	3/2	22 614.85	0.02
442.9446	22 569.87	20 c	5965.45	5/2	28 535.36	7/2	22 569.88	0.03
444.7184	22 479.85	100	5965.45	5/2	28 445.33	5/2	22 479.86	0.02
445.6800	22 431.35	30	1142.79	3/2	23 574.14	5/2	22 431.34	0.01
445.7424	22 428.21	50	1586.90	5/2	24 015.11	7/2	22 428.20	0.01
446.9714	22 366.54	40 c	12 288.25	3/2	34 654.79	5/2	22 366.55	–0.01
447.2536	22 352.43	40 c	2154.11	7/2	24 506.53	9/2	22 352.43	–0.01
450.3040	22 201.01	50	5297.92	3/2	27 498.94	1/2	22 201.01	0.01
452.3409	22 101.04	200	1142.79	3/2	23 243.87	3/2	22 101.04	0.04
454.2797	22 006.72	12 c	0.00	1/2	22 006.74	1/2	22 006.72	0.02
454.6820	21 987.25	120	1586.90	5/2	23 574.14	5/2	21 987.24	0.00
455.3839	21 953.36	30	5965.45	5/2	27 918.85	3/2	21 953.36	0.04
456.4530	21 901.94	60	12 102.12	9/2	34 004.08	11/2	21 901.95	0.01
457.3077	21 861.01	200 c	2154.11	7/2	24 015.11	7/2	21 860.99	0.01
457.4848	21 852.54	25 c	154.19	3/2	22 006.74	1/2	21 852.54	0.01
460.6760	21 701.17	200	2805.36	9/2	24 506.53	9/2	21 701.17	0.00
461.6162	21 656.97	50	1586.90	5/2	23 243.87	3/2	21 656.94	0.03
463.0115	21 591.71	100	11 524.65	13/2	33 116.36	15/2	21 591.72	–0.01
464.8949	21 504.24	100	1142.79	3/2	22 647.03	5/2	21 504.23	0.01
466.3831	21 435.62	100	1586.90	5/2	23 022.56	7/2	21 435.61	0.05

Table 1. continued.

			Lower level		Upper level			
λ_{air}(nm)	$\tilde{\nu}$(cm^{-1})	Int.	E_l(cm^{-1})	J	E_u(cm^{-1})	J	$\tilde{\nu}_{fit}$(cm^{-1})	$\Delta\tilde{\nu}$(cm^{-1})
466.6251*	21 424.50	100	11 247.88	11/2	32 672.39	13/2	21 424.52	–0.01
466.7224†	21 420.03	50	2154.11	7/2	23 574.14	5/2	21 420.03	0.00
467.2097	21 397.69	200 c	2805.36	9/2	24 203.05	11/2	21 397.68	0.01
467.5371	21 382.71	150	2154.11	7/2	23 536.77	9/2	21 382.70	–0.04
468.5133*	21 338.16	100	11 044.08	9/2	32 382.24	11/2	21 338.15	0.02
469.7468	21 282.13	30	8705.32	3/2	29 987.45	5/2	21 282.10	0.03
471.3495	21 209.76	80	2805.36	9/2	24 015.11	7/2	21 209.73	0.02
473.3885	21 118.41	60 c	9043.14	5/2	30 161.56	7/2	21 118.39	0.03
474.3839*	21 074.10	15	8705.32	3/2	29 779.44	3/2	21 074.09	0.03
481.0584	20 781.70	100 c	9497.52	7/2	30 279.23	9/2	20 781.70	0.01
483.3362	20 683.77	40	154.19	3/2	20 837.98	5/2	20 683.77	0.02
484.8359	20 619.79	100 c	9497.52	7/2	30 117.32	9/2	20 619.76	0.04
490.4534	20 383.62	25	0.00	1/2	20 383.62	3/2	20 383.61	0.01
497.1917	20 107.37	10 c	0.00	1/2	20 107.36	1/2	20 107.34	0.02
498.8972	20 038.64	40	695.25	7/2	20 733.88	9/2	20 038.63	0.00
500.0712	19 991.59	4	391.99	5/2	20 383.62	3/2	19 991.63	0.00
501.7743	19 923.74	40	391.99	5/2	20 315.74	7/2	19 923.74	0.01
503.9032	19 839.56	40	154.19	3/2	19 993.78	5/2	19 839.56	0.03
505.7999	19 765.17	40	0.00	1/2	19 765.18	3/2	19 765.17	0.01
506.5256	19 736.85	20	695.25	7/2	20 432.11	9/2	19 736.85	0.01
507.8959	19 683.60	150	1050.26	9/2	20 733.88	9/2	19 683.60	0.02
509.4410*	19 623.90	9 c	0.00	1/2	19 623.96	1/2	19 623.91	0.05
509.5298	19 620.48	80 c	695.25	7/2	20 315.74	7/2	19 620.48	0.01
509.7770	19 610.97	5c	154.19	3/2	19 765.18	3/2	19 610.99	0.00
510.0162	19 601.78	30	391.99	5/2	19 993.78	5/2	19 601.77	0.02
512.0298	19 524.69	20	391.99	5/2	19 916.69	7/2	19 524.68	0.02
512.7662	19 496.65	9	10 126.06	1/2	29 622.73	3/2	19 496.65	0.02
513.4752	19 469.73	40	154.19	3/2	19 623.96	1/2	19 469.73	0.04
515.2623*	19 402.20	12 c	9043.14	5/2	28 445.33	5/2	19 402.20	–0.01
516.4368	19 358.08	40 c	2154.11	7/2	21 512.18	7/2	19 358.07	0.00
518.0306	19 298.52	50	695.25	7/2	19 993.78	5/2	19 298.51	0.02
518.6987	19 273.66	15	154.19	3/2	19 427.90	5/2	19 273.68	0.03
518.9198	19 265.45	20	1050.26	9/2	20 315.74	7/2	19 265.45	0.03
519.3078	19 251.06	40 c	1586.90	5/2	20 837.98	5/2	19 251.07	0.01
519.5839	19 240.83	20	1142.79	3/2	20 383.62	3/2	19 240.83	0.00
520.3224*	19 213.52	10	8705.32	3/2	27 918.85	3/2	19 213.52	0.01
523.7430	19 088.04	16 c	8410.90	1/2	27 498.94	1/2	19 088.04	0.00
525.3926	19 028.11	15	8827.00	7/2	27 855.13	7/2	19 028.10	0.03
526.9910	18 970.39	6	8827.00	7/2	27 797.44	5/2	18 970.39	0.05
527.1526	18 964.58	60 c	1142.79	3/2	20 107.36	1/2	18 964.57	0.00
527.6196	18 947.79	50 c	9497.52	7/2	28 445.33	5/2	18 947.80	0.01
527.9418	18 936.23	8 c	9497.52	7/2	28 433.74	9/2	18 936.20	0.02
531.8597	18 796.74	50	1586.90	5/2	20 383.62	3/2	18 796.73	–0.01
531.9485	18 793.60	15	8705.32	3/2	27 498.94	1/2	18 793.61	0.01
532.0205	18 791.05	3	0.00	1/2	18 791.09	1/2	18 791.04	0.05
533.4864	18 739.42	30	9043.14	5/2	27 782.57	3/2	18 739.42	0.01
533.6797	18 732.63	6	695.25	7/2	19 427.90	5/2	18 732.63	0.02
534.4160	18 706.83	200 c	2805.36	9/2	21 512.18	7/2	18 706.81	0.01
535.0723	18 683.88	100 c	2154.11	7/2	20 837.98	5/2	18 683.85	0.02
539.5849	18 527.62	5	4998.17	1/2	23 525.80	3/2	18 527.61	0.02
539.633	18 525.97	7 c	8410.90	1/2	26 936.86	3/2	18 525.95	0.01
543.125	18 406.86	12 d	1586.90	5/2	19 993.78	5/2	18 406.86	0.02
543.7265*	18 386.50	50	5297.92	3/2	23 684.44	5/2	18 386.50	0.02
550.458	18 161.66	30 c	2154.11	7/2	20 315.74	7/2	18 161.62	0.01
551.281	18 134.54	15 c	2805.36	9/2	20 939.92	11/2	18 134.51	0.05
555.134 *	18 008.68	60	4998.17	1/2	23 006.86	3/2	18 008.63	0.06
558.699	17 893.77	30	1142.79	3/2	19 036.55	3/2	17 893.75	0.01
560.351	17 841.02	30	1586.90	5/2	19 427.90	5/2	17 840.98	0.02
562.825	17 762.59	10 c	2154.11	7/2	19 916.69	7/2	17 762.56	0.02
562.917	17 759.69	40	12 357.70	9/2	30 117.32	9/2	17 759.67	–0.05
564.210	17 718.99	80	5965.45	5/2	23 684.44	5/2	17 718.94	0.05
566.470	17 648.30	100	1142.79	3/2	18 791.09	1/2	17 648.26	0.04
566.563 *	17 645.40	120	13 012.20	11/2	30 657.60	11/2	17 645.39	0.01
567.190	17 625.90	50	12 136.86	7/2	29 762.70	7/2	17 625.85	–0.01
569.307 *	17 560.35	8	5965.45	5/2	23 525.80	3/2	17 560.32	0.03

Table 1. continued.

			Lower level		Upper level			
λ_{air}(nm)	$\tilde{\nu}$(cm^{-1})	Int.	E_l(cm^{-1})	J	E_u(cm^{-1})	J	$\tilde{\nu}_{fit}$(cm^{-1})	$\Delta\tilde{\nu}$(cm^{-1})
570.647	17 519.12	50	8410.90	1/2	25 930.01	3/2	17 519.11	0.00
572.9185	17 449.66	80	1586.90	5/2	19 036.55	3/2	17 449.65	0.00
575.143	17 382.17	40	12 136.86	7/2	29 519.05	9/2	17 382.16	0.03
576.033	17 355.31	80	8705.32	3/2	26 060.65	5/2	17 355.30	0.03
578.752	17 273.78	80	2154.11	7/2	19 427.90	5/2	17 273.76	0.03
580.402	17 224.67	30 d	8705.32	3/2	25 930.01	3/2	17 224.68	0.01
581.9415*	17 179.11	80 d	13 012.20	11/2	30 191.25	13/2	17 179.07	–0.02
583.488 *	17 133.57	40	13 145.71	9/2	30 279.23	9/2	17 133.56	–0.04
583.813	17 124.04	15 c	11 318.09	3/2	28 442.16	1/2	17 124.04	0.03
583.861	17 122.63	100 c	9043.14	5/2	26 165.79	7/2	17 122.60	0.05
584.247	17 111.32	30	2805.36	9/2	19 916.69	7/2	17 111.30	0.03
586.645	17 041.37	80	5965.45	5/2	23 006.86	3/2	17 041.34	0.07
587.468	17 017.50	40 c	9043.14	5/2	26 060.65	5/2	17 017.48	0.03
590.059	16 942.77	200 c	9497.52	7/2	26 440.33	9/2	16 942.77	0.04
598.321	16 708.82	100	5297.92	3/2	22 006.74	1/2	16 708.80	0.02
598.608	16 700.81	30	13 145.71	9/2	29 846.50	11/2	16 700.79	0.00
666.084	15 008.98	300 c	9497.52	7/2	24 506.53	9/2	15 008.98	0.03
667.734	14 971.90	200 c	9043.14	5/2	24 015.11	7/2	14 972.02	–0.05
670.120 *	14 918.59	60	13 515.20	7/2	28 433.74	9/2	14 918.57	–0.03
672.362	14 868.84	150	8705.32	3/2	23 574.14	5/2	14 868.80	0.02
673.988	14 832.97	80	8410.90	1/2	23 243.87	3/2	14 832.92	0.05
682.811	14 641.31	150	9043.14	5/2	23 684.44	5/2	14 641.27	0.03
690.289	14 482.70	50 c	9043.14	5/2	23 525.80	3/2	14 482.65	0.01
699.032 *	14 301.56	100	8705.32	3/2	23 006.86	3/2	14 301.50	0.04
704.681	14 186.92	300 c	9497.52	7/2	23 684.44	5/2	14 186.87	0.05
715.944	13 963.73	100	9043.14	5/2	23 006.86	3/2	13 963.68	0.04
725.235	13 784.81	40	10 126.06	1/2	23 910.90	1/2	13 784.80	0.04
737.251	13 560.17	500	11 344.70	5/2	24 904.86	7/2	13 560.16	0.00
757.457	13 198.44	500	11 344.70	5/2	24 543.13	5/2	13 198.41	0.02
772.667	12 938.63	100	11 344.70	5/2	24 283.34	3/2	12 938.61	0.03

Notes. Wavelength in air λ_{air}, wavenumbers $\tilde{\nu}$, intensities, and level energies E according to Humphreys & Meggers (1945), centre of gravity $\tilde{\nu}_{fit}$ resulting from the hyperfine structure fit and $\Delta\tilde{\nu} = E_u - E_l - \tilde{\nu}_{fit}$.
(†) Wrong classification given in Humphreys & Meggers (1945); (*) FWHM and ratio between Gaussian and Lorentzian FWHM fixed during the fit; r: self-reversal line; c: complex line; d: double line.

constant of the lower level was used instead of the standard deviation.

4. Results and discussion

In total, 224 spectral lines were investigated (see Table 1). For all lines except one (marked with the symbol † in Table 1) the classification given in Humphreys & Meggers (1945) was confirmed. The spectral profiles of all lines were fitted in order to obtain the magnetic dipole hyperfine constants A of the upper levels, which were the levels of odd parity in all cases. The resulting 109 hyperfine structure constants A are listed in Table 3, sorted by level energies.

The hyperfine structure constants A_{fit} given in the fifth column of Table 3 are the statistical mean value of the eight measurements, the measurement uncertainty ΔA_{fit} in the sixth column being the corresponding standard deviation. These errors refer only to the statistical variation of the fit and do not include systematic errors, which may occur, for example, because of neglecting the electric quadrupole hyperfine structure constant B or as a result of other restrictions in the fit. This implies that the measurement uncertainty ΔA_{fit} may be sometimes too small. This was the case when the hyperfine structure constants A_{fit} for one level, determined from different lines, did not agree with each other within the limits of measurement uncertainty (see, for example, the level 25 199.81 cm^{-1}). Nevertheless, the value of ΔA_{fit} conveys an idea about the accuracy of the A_{fit} value. If the measurement uncertainty of the hyperfine constant A_l of the lower level, which was fixed during the fit (see Sect. 3), was higher than the standard deviation, it is given as measurement uncertainty ΔA_{fit} in column six (and is marked by the symbol ‡).

In the fourth column of Table 3 the transitions are listed that were used to determine the A_{fit} value. If the hyperfine structure constant A of a level of odd parity was measured in different transitions, the weighted mean value A_{mean} is taken, weighted by the measurement uncertainty of column six. These values are listed in column seven. The measurement uncertainties given for the mean values A_{mean} are the standard deviations corresponding to this average. They are much more significant than the ΔA_{fit} values, particularly if more than two lines were used. For hyperfine constants measured from only one transition, no measurement uncertainty is indicated in column seven.

The FWHM values of the Voigt profile determined from the hyperfine structure fits are shown in Fig. 5 as function of the transition wavenumber, together with the FWHM values corresponding to the Lorentzian and Gaussian parts of the Voigt profile function. For each of the three data sets a linear fit is added to the graph. The results of these linear fits are listed in Table 4. The FWHM of the Gaussian part has nearly the same slope as the FWHM of the Voigt profile whereas the FWHM of the Lorentzian part is nearly independent of the transition wave number.

Table 2. Hyperfine structure constants A_l and B_l from the literature for low-lying levels of even parity.

E(cm^{-1})	Configuration	Term	Method	A_l(MHz)	B_l(MHz)	Ref.
0.00	$4d^45s$	$^6D_{1/2}$	abmr	1868.2184 (18)	–	Büttgenbach et al. (1975)
154.19	$4d^45s$	$^6D_{3/2}$	abmr	852.5428 (21)	–64.572 (41)	Büttgenbach et al. (1975)
391.99	$4d^45s$	$^6D_{5/2}$	abmr	719.4759 (18)	–47.605 (39)	Büttgenbach et al. (1975)
695.25	$4d^45s$	$^6D_{7/2}$	abmr	690.1978 (16)	20.475 (75)	Büttgenbach et al. (1975)
1050.26	$4d^45s$	$^6D_{9/2}$	abmr	691.6141 (22)	132.754 (116)	Büttgenbach et al. (1975)
1142.79	$4d^35s^2$	$^4F_{3/2}$	abmr	644.16 (54)	32.800 (128)	Büttgenbach et al. (1975)
1 586.90	$4d^35s^2$	$^4F_{5/2}$	abmr	372.4853 (17)	33.341 (38)	Büttgenbach et al. (1975)
2154.11	$4d^35s^2$	$^4F_{7/2}$	abmr	292.2022 (16)	44.928 (47)	Büttgenbach et al. (1975)
2805.36	$4d^35s^2$	$^4F_{9/2}$	abmr	269.6320 (26)	64.315 (130)	Büttgenbach et al. (1975)
4998.17	$4d^35s^2$	$^4P_{1/2}$	lrf	540.1 (0.9)	–	Fraenkel et al. (1988)
5297.92	$4d^35s^2$	$^4P_{3/2}$	lrf	497.7569 (16)	59.902 (14)	Fraenkel et al. (1988)
5965.45	$4d^35s^2$	$^4P_{5/2}$	lrf	343.1670 (5)	–80.454 (9)	Fraenkel et al. (1988)
8410.90	$4d^45s$	$^4D_{1/2}$	lrf	1997.0 (1.1)	–	Fraenkel et al. (1988)
8705.32	$4d^45s$	$^4D_{3/2}$	lrf	–143.3225 (217)	–10.761 (178)	Fraenkel et al. (1988)
8827.00	$4d^35s^2$	$^2G_{7/2}$	lrf	420.2938 (11)	–49.006 (36)	Fraenkel et al. (1988)
9043.14	$4d^45s$	$^4D_{5/2}$	lrf	–407.8606 (43)	35.060 (75)	Fraenkel et al. (1988)
9328.88	$4d^35s^2$	$^2G_{9/2}$	lrf	358.5642 (8)	–61.048 (30)	Fraenkel et al. (1988)
9439.08	$4d^35s^2$	$^2D_{3/2}$	lrf	389.1039 (23)	73.590 (19)	Fraenkel et al. (1988)
9497.52	$4d^45s$	$^4D_{7/2}$	lrf	–477.0373 (35)	126.899 (81)	Fraenkel et al. (1988)
10 126.06	$4d^35s^2$	$^2P_{1/2}$	lrf	323.6590 (4)	–	Fraenkel et al. (1988)
10 237.51	$4d^35s^2$	$^2D_{5/2}$	lrf	295.6803 (6)	36.501 (12)	Fraenkel et al. (1988)
10 922.74	$4d^45s$	$^4H_{7/2}$	lif	–200 (50)	–	Kröger (2007)
11 044.08	$4d^45s$	$^4H_{9/2}$	lif	334 (50)	–	Kröger (2007)
11 247.88	$4d^45s$	$^4H_{11/2}$	lif	560 (30)	–	Kröger (2007)
11 344.70	$4d^5$	$^6S_{5/2}$	lrf	–639.3786 (79)	–0.061 (92)	Fraenkel et al. (1988)
11 524.65	$4d^45s$	$^4H_{13/2}$	lif	662 (20)	–	Kröger (2007)
12 102.12	$4d^35s^2$	$^2H_{9/2}$	lrf	384.9669 (33)	–163.323 (96)	Fraenkel et al. (1988)
12 136.86	$4d^45s$	$^4G_{7/2}$	lif	502.4 (1.4)	–	Kröger (2007)
12 288.25	$4d^45s$	$^4F_{3/2}$	ogs	–592 (2)	–	Başar et al. (2008)
13 012.20	$4d^45s$	$^4G_{11/2}$	ogs	699 (5)	–	Başar et al. (2008)
13 515.20	$4d^35s^2$	$^2F_{7/2}$	lrf	136.9050 (6)	–48.916 (14)	Fraenkel et al. (1988)

Notes. abmr – atomic beam magnetic resonance technique, lrf – laser radio-frequency double resonance, lif – laser induced fluorescence spectroscopy, ogs – optogalvanic spectroscopy.

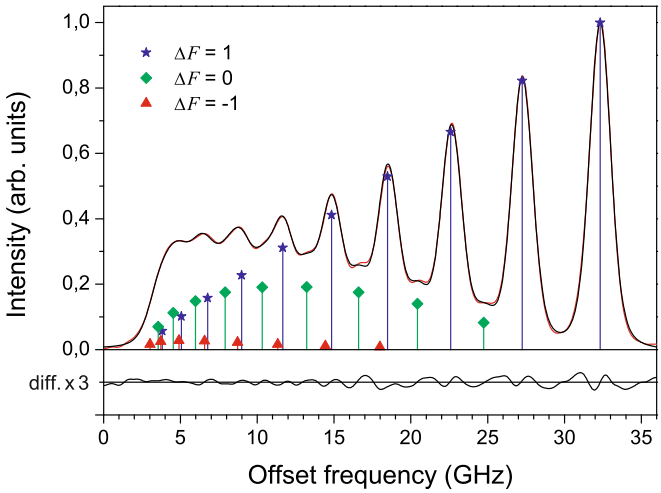

Fig. 3. Example of a partially resolved line: Fourier transform spectrum of the transition 24 203.05 cm^{-1} (J = 11/2) ⟶ 2805.36 cm^{-1} (J = 9/2) at λ_{air} = 467.2097 nm together with the best fitted curve. In the lower part of the figure, the residuals between the experiment and the fit are given, multiplied by a factor of 3. The components were assigned by the difference ΔF of the total angular momentum of the upper and lower hyperfine levels.

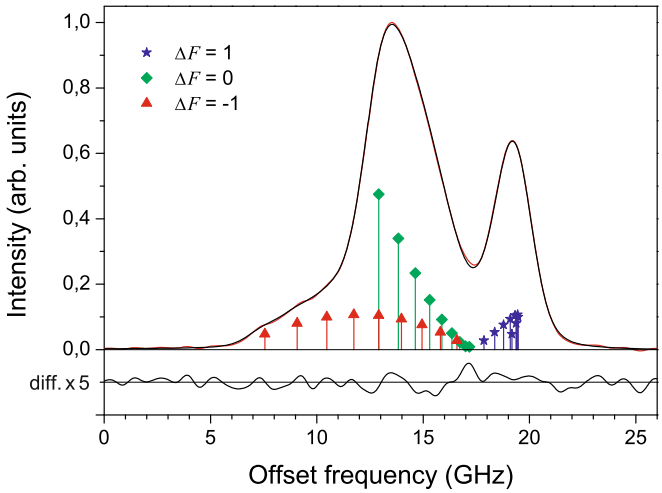

Fig. 4. Example of an unresolved line: Fourier transform spectrum of the transition 24 506.53 cm^{-1}, J = 9/2 ⟶ 1050.26 cm^{-1}, J = 9/2 at λ_{air} = 426.2056 nm together with the best fitted curve. In the lower part of the figure, the residuals between the experiment and the fit are given, multiplied by a factor of 5. The components were assigned by the difference ΔF of the total angular momentum of the upper and lower hyperfine levels.

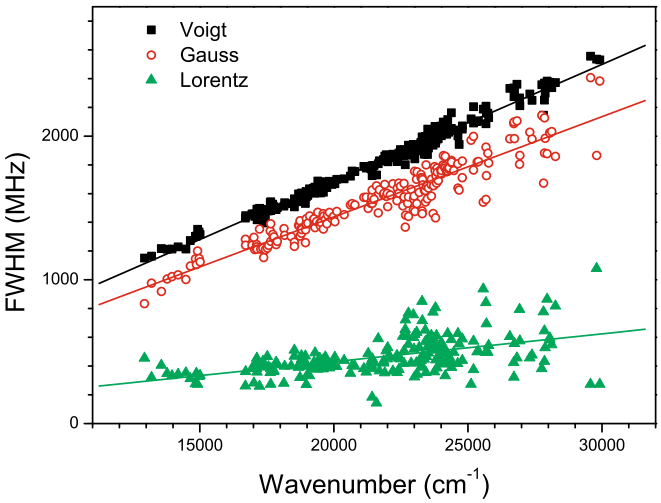

Fig. 5. FWHM as a function of the transition wavenumber for the Voigt profile as well as for the Lorentzian and the Gaussian parts that resulted from the fit of the hyperfine structure together, fitted in each case by straight lines. All investigated lines are recorded except those for which the FWHM had been fixed during the fit.

For some unresolved lines the Voigt FWHM deviated strongly from the trend line FWHM($\tilde{\nu}$) in Fig. 5. If this deviation was more than 200 MHz, the FWHM and the profile parameter were fixed during the fit to the value of the trend line at the corresponding wave number. These transitions are marked by asterisks in Tables 1 and 3. The FWHM values of these lines are excluded from the plot in Fig. 5.

The Gaussian portion of the linewidth results from the Doppler broadening in the hollow cathode lamp and varies between 950 MHz for small wavenumber values and 2000 MHz for large wavenumber values. The respective straight line from the linear fit goes through the origin of the graph (intercept the wavenumber axis at zero), which is in good agreement with the formula for the FWHM of a Doppler broadened line

$$\Delta\nu_{\mathrm{Doppler}} = \tilde{\nu}\sqrt{\frac{8k_{\mathrm{B}}T\ln 2}{m}}, \qquad (2)$$

where T is the temperature, k_{B} is the Boltzmann constant and m is the mass of the emitting particle (92.906 au for ^{93}Nb). From the values of the Gaussian FWHM, the corresponding temperature in the hollow cathode discharge can be determined. The temperature values calculated for all lines were independent of the wave number (as they should be) and showed statistical variations only. Averaging over all lines leads to a temperature of 1050 (100) K.

The Lorentzian part mainly reflects the apparatus function of the FT spectrometer which was approximately 600 MHz for our resolution. The natural linewidth for the lines under investigation is significantly less than 600 MHz, and its contribution is small.

A further parameter resulting from the fit is the centre of gravity of the hyperfine structure $\tilde{\nu}_{\mathrm{fit}}$, i.e., the centre of gravity of a line. The mean values of the eight fits for $\tilde{\nu}_{\mathrm{fit}}$ are listed in the penultimate column of Table 1. The standard deviation of $\tilde{\nu}_{\mathrm{fit}}$ was on average 0.002 cm^{-1} and always smaller than 0.01 cm^{-1}. To check the consistency of the fine structure levels, the differences $\Delta\tilde{\nu} = E_u - E_l - \tilde{\nu}_{\mathrm{fit}}$ were calculated and listed in the last column of Table 1. All values of $\Delta\tilde{\nu}$ were smaller than 0.07 cm^{-1}, and the average of the absolute value of $\Delta\tilde{\nu}$ was 0.02 cm^{-1}. This confirms the fine structure level energies given in Humphreys & Meggers (1945).

The existing experimental values of the hyperfine constants from the literature, together with the specification of the experimental methods used, are given in the last two columns of Table 3. If more than one reference value has been published for a given level, only the most precise one is given.

The A values of 57 levels were measured for the first time. For the other 52 levels our values agree mostly with the previous values within the measurement uncertainty. For a few A values the difference between the A_{mean} and the A_{ref} values were slightly outside of the measurement uncertainty, exceeding it by ca. 50%. Only for two levels our new A values lie noticeably outside of the measurement uncertainty of the previous values which were determined by Singh et al. (1992). For these levels, 31 174.65 cm^{-1} and 35 156.94 cm^{-1}, our A values were measured from only one line in each case. For the level 31 174.65 cm^{-1} the disagreement between our A value and the reference one was 64 MHz. Singh et al. (1992) used the line at 589.34 nm to determine the A value. However, the constant A_l of the lower level of this line was already the subject of discussion in Bouzed et al. (2003), and it was considered to be wrong because it differed by more than 700 MHz from a more recent A_l value. For this reason we assume the reference value A of the level 31 174.65 cm^{-1} to be incorrect and trust our value as much as all other unconfirmed A values measured with only one line. The disagreement for the second level 35 156.94 cm^{-1} was 122.5 MHz. Neither our value nor the value from Singh et al. (1992) are confirmed by another measurement.

5. Astrophysical interest

A reliable abundance of niobium in the solar photosphere was determined by Hannaford et al. (1985) using original radiative lifetimes of Nb II lines. Equivalent widths of 11 Nb II lines were measured in the solar spectrum to calculate the niobium abundance, $A_{\mathrm{Nb}} = \log(N_{\mathrm{Nb}}/N_{\mathrm{H}}) + 12.00 = 1.42 \pm 0.06$. The hyperfine structure splitting was neglected in those estimates. The latest review of the standard solar composition (SAD) recommends the value $A_{\mathrm{Nb}} = 1.39 \pm 0.03$ (Grevesse et al. 2007), which is in good agreement with the meteoritic abundance. Kwiatkowski et al. (1982) obtained a much higher solar niobium abundance $A_{\mathrm{Nb}} = 2.10 \pm 0.10$, using Nb I lines. The most plausible explanation of such a discrepancy seems to be the uncertainty in measurements of equivalent widths for weak and broad Nb I absorption lines disturbed by hyperfine splitting. Thus, the hyperfine structure can have a significant effect on stellar absorption line profiles and the corresponding abundances can be substantially overestimated if such effects are not taken into account in the calculations (Booth & Blackwell 1983). Therefore, a detailed consideration of hyperfine structure is important for stellar abundance determinations.

The chemical elements heavier than iron are created by a combination of slow (s) and rapid (r) neutron-capture nucleosynthesis processes (Burbidge et al. 1957). The theory of nucleosynthesis identifies different astrophysical sites for s- and r-processes. The r-process nuclei are the products formed primarily during the evolution of massive stars and supernova explosions. The s-process nuclei are generally thought to have been synthesized during the late stages of the stellar evolution of low mass stars. Recent studies argue about two separate r-processes responsible for the production of the heavier and lighter neutron capture elements (Sneden et al. 2008, and references therein). The detection of lighter neutron capture elements ($38 \le Z \le 48$)

Table 3. Magnetic dipole hyperfine structure constants A in MHz for the levels of odd parity of Nb I.

E(cm^{-1})	Config.	Term	λ_{air}(nm)	A_{fit}	ΔA_{fit}	A_{mean}	A_{ref}	Ref.
18 791.09	4d^{3}5s5p	$^6F_{1/2}$	566.470	–788.5	0.6			
			532.0205	–784.7	12.4	–788.5 (2)	–779. 6(10.0)	Singh & Rao (1989)[a]
19 036.55			572.9185	539.0	2.7			
			558.699	539.3	1.2	539.3 (1)		
19 427.90	4d^{3}5s5p	$^6F_{5/2}$	578.752	662.6	0.5			
			560.351	663.2	0.7			
			533.6797	662.7	2.6			
			518.6987	662.7	0.5	662.8 (1)	654.7 (10.0)	Singh & Rao (1989)[a]
19 623.96	4d^{3}5s5p	$^6D_{1/2}$	513.4752	1713.5	0.4			
			509.4410*	1715.0	2.8	1713.5 (2)		
19 765.18	4d^{3}5s5p	$^6D_{3/2}$	509.7770	926.6	4.7			
			505.7999	923.9	0.3	923.9 (2)		
19 916.69	4d^{3}5s5p	$^6F_{7/2}$	584.247	667.1	0.9			
			562.825	667.4	2.8			
			512.0298	667.8	0.1	667.8 (1)	680.6 (10.0)	Singh & Rao (1989)[a]
19 993.78	4d^{3}5s5p	$^6D_{5/2}$	543.125	828.7	2.1			
			518.0306	826.1	0.4			
			510.0162	828.3	0.5			
			503.9032	828.3	0.3	827.7 (6)	827 (3)	Kröger (2007)[a]
20 107.36	4d^{3}5s5p	$^4D_{1/2}$	527.1526	–794.8	0.7			
			497.1917	–792.5	3.4	–794.7 (5)	–792 (3)[†]	Başar et al. (2008)[a]
20 315.74	4d^{3}5s5p	$^6D_{7/2}$	550.458	786.1	1.4			
			518.9198	784.7	0.6			
			509.5298	786.2	0.1			
			501.7743	785.9	0.2	786.1 (1)	786 (5)	Kröger (2007)[a]
20 383.62	4d^{3}5s5p	$^4D_{3/2}$	531.8597	597.2	3.3			
			519.5839	597.5	0.7			
			500.0712	599.2	4.3			
			490.4534	595.0	3.4	597.4 (3)	597.8 (5)	Başar et al. (2008)[b]
20 432.11			506.5256	693.9	0.2	693.9		
20 733.88	4d^{3}5s5p	$^6D_{9/2}$	507.8959	734.3	0.2			
			498.8972	733.6	0.2	733.9 (4)		
20 837.98	4d^{3}5s5p	$^4D_{5/2}$	535.0723	809.8	0.3			
			519.3078	809.7	0.4			
			483.3362	810.0	0.6	809.8 (1)	808.8 (4)	Başar et al. (2008)[b]
20 939.92	4d^{3}5s5p	$^6F_{11/2}$	551.281	755.5	0.9	755.5	756 (4)	Kröger (2007)[c]
21 512.18	4d^{3}5s5p	$^4D_{7/2}$	534.4160	872.6	0.2			
			516.4368	872.6	0.5	872.6 (0)	872.8 (5)	Başar et al. (2008)[b]
22 006.74	4d^{4}5p	$^4P_{1/2}$	598.321	–269.7	2.2			
			457.4848	–265.5	2.7			
			454.2797	–265.2	11.9	–268 (2)	–267.3 (3)	Fraenkel et al. (1988)[d]
22 647.03	4d^{3}5s5p	$^4G_{5/2}$	464.8949	–78.5	0.2	–78.5		
23 006.86	4d^{4}5p	$^4P_{3/2}$	715.944	–140.6	4.0			
			699.032*	–138.2	2.6			
			586.645	–139.9	1.0			
			555.134*	–138.4	0.7			
			442.0637	–139.7	2.0			
			434.5315	–138.1	2.5	–138.9 (3)	–137.9 (4)	Fraenkel et al. (1988)[d]
23 022.56	4d^{3}5s5p	$^4G_{7/2}$	466.3831	430.3	0.2	430	430 (40)	Kröger (2007)[a]
23 243.87	4d^{3}5s5p	$^4F_{3/2}$	673.988	–17.1	2.1			
			461.6162	–15.4	1.5			
			452.3409	–16.7	0.5			
			432.9732	–11.8	5.1	–16.6 (3)	0 (30)	Kröger (2007)[a]
23 525.80	4d^{3}5s5p	$^2D_{3/2}$	690.289	596.9	7.0			
			569.307*	595.7	2.1			
			539.5849	593.6	2.9			
			424.9457	593.4	2.7	594.6 (7)	595 (7)	Kröger (2007)[a]
23 536.77	4d^{3}5s5p	$^4G_{9/2}$	467.5371	632.6	0.1	633		
23 574.14	4d^{3}5s5p	$^4F_{5/2}$	672.362	514.7	1.6			
			466.7224	515.4	1.0			
			454.6820	514.6	0.3			
			445.6800	514.6	1.3			
			431.2454	517.2	2.3			
			426.8667	516.7	11.7	514.7 (2)	514.1 (2)	Başar et al. (2008)[b]

Table 3. continued.

E(cm^{-1})	Config.	Term	λ_{air}(nm)	A_{fit}	ΔA_{fit}	A_{mean}	A_{ref}	Ref.
23 684.44	4d^{4}5p	^{6}P$_{5/2}$	704.681	104.1	0.9			
			682.811	103.4	1.8			
			564.210	102.4	1.2			
			543.7265*	104.7	4.5			
			434.8652	101.8	2.2			
			429.2035	104.7	2.0	103.5 (4)		
23 910.90	4d^{3}5s5p	^{2}S$_{1/2}$	725.235	626.8	3.4			
			420.8156	625.6	4.2	626.3 (6)	627.4 (6)	Başar et al. (2008)[b]
23 984.87	4d^{4}5p	^{6}F$_{1/2}$	419.5096	1469.9	6.2			
			416.8122	1474.4	0.8	1474.3 (6)		
24 015.11	4d^{3}5s5p	^{4}F$_{7/2}$	667.734	592.7	1.2			
			471.3495	592.3	1.2			
			457.3077	592.0	0.3			
			445.7424	592.2	2.2			
			435.3266	595.0	5.4			
			428.6987	592.9	0.8			
			423.1954	592.8	3.1	592.2 (1)	591.8 (3)	Başar et al. (2008)[b]
24 164.79	4d^{4}5p	^{6}F$_{3/2}$	420.5308	269.5	3.5			
			416.3658	266.4	0.7			
			413.7090*	267.5	0.8	266.9 (5)		
24 203.05	4d^{3}5s5p	^{4}G$_{11/2}$	467.2097	752.3	0.1	752		
24 283.34	4d^{4}5p	^{6}P$_{3/2}$	772.667	91.4	6.8			
			418.4440	93.0	2.9			
			414.3201	90.8	1.7			
			411.6895	90.6	1.0	90.9 (4)	93 (1)	Başar et al. (2008)[a]
24 396.80	4d^{4}5p	^{6}F$_{5/2}$	421.7946	228.8	3.0			
			416.4661	227.5	0.3			
			412.3812	227.1	1.1	227.5 (1)	227.6 (6)	Başar et al. (2008)[a]
24 506.53	4d^{3}5s5p	^{4}F$_{9/2}$	666.084	597.3	0.7			
			460.6760	593.6	0.2			
			447.2536	593.9	1.2			
			426.2056	594.0	0.6			
			419.8510	591.9	1.1	593.8 (5)	593.0 (4)	Başar et al. (2008)[b]
24 543.13	4d^{4}5p	^{6}P$_{5/2}$	757.457	137.5	2.2			
			419.2065	136.6	0.7			
			413.9430	137.1	1.3			
			409.9067	136.9	1.6	136.8 (2)		
24 769.91	4d^{4}5p	^{6}F$_{7/2}$	421.4732	138.0	4.4			
			415.2575	139.3	0.5			
			410.0918	138.3	0.3	138.6 (3)		
24 773.03	4d^{3}5s5p	^{2}D$_{1/2}$	415.2040	168.9	4.7			
			410.0389	171.4	1.5			
			406.0800	169.8	2.1	170.7 (6)	170.1 (5)	Başar et al. (2008)[b]
24 904.86	4d^{4}5p	^{6}P$_{7/2}$	737.251	195.7	1.7			
			419.0889	194.7	0.6			
			412.9430	194.3	1.0	194.7 (3)		
25 199.81	4d^{4}5p	^{6}F$_{9/2}$	413.9702	113.1	0.4			
			407.9726*	112.2	0.2	112.4 (4)		
25 680.36	4d^{4}5p	^{6}F$_{11/2}$	405.8933*	44.9	0.1	45		
25 930.01	4d^{4}5p	^{4}F$_{3/2}$	580.402	558.6	6.6			
			570.647	559.4	1.1			
			403.3195	560.7	1.8	559.7 (4)	557.4 (5)	Fraenkel et al. (1988)[d]
26 060.65	4$d^4$5p	$^4F_{5/2}$	587.468	266.6	2.2			
			576.033	264.9	1.7			
			408.4861	269.0	4.0	265.9 (9)	266.7 (3)	Fraenkel et al. (1988)[d]
26 067.06	4d^{3}5s5p	^{6}D$_{3/2}$	389.3733	933.2	13.4	933	943.5 (1.8)	Bouzed et al. (2003)[c]
26 165.79	4d^{4}5p	^{4}F$_{7/2}$	583.861	297.9	1.1			
			416.3474	298.0	0.9			
			398.0483*	293.6	3.5			
			387.8817	294.9	2.3	297.6 (7)	299.6 (10.0)	Singh & Rao (1989)[a]
26 386.36	4d^{3}5s5p	^{6}D$_{5/2}$	389.1302	804.1	6.4	804	809.2 (5)	Fraenkel et al. (1988)[d]
26 440.33	4d^{4}5p	^{4}F$_{9/2}$	590.059	339.6	1.6			
			422.9832	334.8	1.5			
			393.7437	337.8	0.8			
			388.3141	336.1	2.1	337.4 (8)	337.6 (2)	Fraenkel et al. (1988)[d]

Table 3. continued.

E(cm^{-1})	Config.	Term	λ_{air}(nm)	A_{fit}	ΔA_{fit}	A_{mean}	A_{ref}	Ref.
26 713.32	4d^{4}5p	^{6}D$_{3/2}$	374.2393	103.6	4.6	104	108.6 (4)	Fraenkel et al. (1988)[d]
26 717.73	4d^{3}5s5p	^{4}D$_{1/2}$	390.8971	501.2	6.3			
			376.3492	512.3	7.6			
			374.1776*	510.5	11.6	506 (4)	508.3 (4)	Fraenkel et al. (1988)[d]
26 936.86	4d^{4}5p	^{6}D$_{3/2}$	539.633	39.1	7.7			
			394.3663	41.4	5.0			
			371.1343	39.6	2.8	39.9 (6)		
26 983.34	4d^{4}5p	^{6}D$_{5/2}$	372.6235	196.4	3.5	196		
27 359.70	4d^{4}5p	^{4}D$_{5/2}$	396.6246	–22.4	1.2	–22	–25.5 (2.0)	Başar et al. (2008)[a]
27 427.07	4d^{4}5p	^{6}D$_{7/2}$	373.9800	384.7	2.2	385	386.0 (5)	Fraenkel et al. (1988)[d]
27 498.94	4d^{4}5p	^{4}P$_{1/2}$	531.9485	929.5	18.5			
			523.7430	920.9	12.6			
			450.3040	924.8	6.8	925 (2)		
27 596.74	4d^{4}5p	^{4}D$_{7/2}$	403.2524	–144.0	0.4	–144	–149 (2)	Başar et al. (2008)[a]
27 666.46	4d^{3}5s5p	^{4}D$_{1/2}$	441.0214	729.7	2.3	730	726 (4)	Başar et al. (2008)[a]
27 782.57	4d^{4}5p	^{4}P$_{3/2}$	533.4864	596.1	5.5			
			438.7743	597.6	6.4			
			364.9854	593.9	3.6	595 (1)		
27 797.44			526.9910	568.4	4.9	568		
27 855.13			525.3926	438.4	1.4	438	439.1 (7)	Kröger (2007)[a]
27 918.85	4d^{4}5p	^{4}D$_{3/2}$	520.3224*	347.7	4.4			
			455.3839	351.1	8.9			
			441.9448	345.2	7.2	348 (1)		
27 974.87	4d^{3}5s5p	^{6}D$_{9/2}$	371.3018	525.1	0.4			
			366.4692*	525.7	3.2	525.1 (1)	504 (15)	Başar et al. (2008)[a]
28 079.09	4d^{3}5s5p	^{4}P$_{3/2}$	438.8357	675.3	5.3			
			433.1371	676.3	1.6	676.2 (3)	678 (6)	Başar et al. (2008)[a]
28 208.48	4d^{3}5s5p	^{4}P$_{3/2}$	359.3966*	957.8	8.5			
			356.3501	943.6	2.1	944 (3)		
28 278.25	4d^{3}5s5p	^{6}P$_{3/2}$	358.4972	733.7	8.3			
			355.4666*	750.5	3.8	748 (6)	747.1 (8)	Fraenkel et al. (1988)[d]
28 433.74	4d^{3}5s5p	^{2}G$_{9/2}$	670.120 *	179.5	1.1			
			527.9418	180.2	2.9	179.6 (2)	179.5 (4)	Başar et al. (2008)[b]
28 442.16	4d^{3}5s5p	^{2}P$_{1/2}$	583.813	2239.5	19.3	2240	2242.7 (1.2)	Fraenkel et al. (1988)[d]
28 445.33	4d^{3}5s5p	^{4}P$_{5/2}$	527.6196	611.8	2.5			
			515.2623*	610.9	5.9			
			444.7184	616.2	2.4			
			360.2561	611.8	5.0			
			356.3624	620.1	5.2	614 (1)	607.8 (6.0)	Singh et al. (1992)[a]
28 535.36	4d^{3}5s5p	^{4}D$_{7/2}$	442.9446	660.5	0.9	661	662 (3)	Bouzed et al. (2003)[a]
28 549.42	4d^{3}5s5p	^{4}P$_{5/2}$	429.9596	677.3	0.9			
			358.9106	675.1	1.8	676.9 (9)		
28 652.66	4d^{3}5s5p	^{6}P$_{5/2}$	357.5850	752.8	1.5			
			353.7475	762.8	5.3	754 (3)	746.2 (6.0)	Singh et al. (1992)[a]
28 973.12	4d^{3}5s5p	^{6}P$_{7/2}$	358.0277*	599.1	1.7	599		
29 209.42	4d^{3}5s5p	^{4}D$_{7/2}$	430.0989	523.9	0.7	524	505.4 (6.0)	Singh et al. (1992)[a]
29 271.99	4d^{3}5s5p	^{4}H$_{7/2}$	428.9443	189.1	0.9	189	189.5 (3)	Fraenkel et al. (1988)[d]
29 519.05	4d^{3}5s5p	^{4}H$_{9/2}$	575.143	413.0	3.4	413		
29 622.73	4d^{3}5s5p	^{2}D$_{3/2}$	512.7662	181.8	6.2	182		
29 762.70	4d^{3}5s5p	^{4}F$_{7/2}$	567.190	374.3	1.4‡			
			362.1030*	378.1	2.9	375 (2)		
29 779.44	4d^{3}5s5p	^{4}F$_{3/2}$	474.3839*	–19.8	5.6	–20		
29 846.50	4d^{3}5s5p	^{4}H$_{11/2}$	598.608	539.8	0.8	540		
29 987.45	4d^{3}5s5p	^{4}F$_{5/2}$	469.7468	476.5	3.3	477		
30 117.32	4d^{3}5s5p	^{4}F$_{9/2}$	562.917	620.2	1.3			
			484.8359	618.3	1.1			
			366.0364	620.0	1.3	619.4 (6)	622 (5)	Başar et al. (2008)[a]
30 161.56	4d^{3}5s5p	^{4}F$_{7/2}$	473.3885	516.4	2.4	516		
30 191.25	4d^{3}5s5p	^{4}H$_{13/2}$	581.9415*	565.7	5‡	566		
30 279.23	4d^{4}5p	^{4}F$_{9/2}$	583.488 *	604.8	1.3			
			481.0584	601.6	2.6			
			355.4524*	597.5	4.2	604 (2)		
30 657.60	4d^{3}5s5p	^{4}G$_{11/2}$	566.563*	684.4	5‡			
			358.9356	701.2	2.0	699 (6)		

Table 3. continued.

E(cm^{-1})	Config.	Term	λ_{air}(nm)	A_{fit}	ΔA_{fit}	A_{mean}	A_{ref}	Ref.
30 716.50	4d^{3}5s5p	^{2}F$_{5/2}$	338.0420*	476.9	13.3	477	477.8 (4)	Fraenkel et al. (1988)[d]
31 056.60	4d^{3}5s5p	^{4}G$_{5/2}$	334.1982*	915.3	7.7	915		
31 174.65	4d^{3}5s5p	^{4}S$_{3/2}$	396.5692	1111.1	11.8	1111	1047.0 (6.0)	Singh et al. (1992)[a]
31 485.20	4d^{3}5s5p	^{4}G$_{7/2}$	334.3712*	337.1	6.4	337		
31 707.94	4d^{3}5s5p	^{4}D$_{3/2}$	429.1195*	561.1	8.2	561		
31 800.74	4d^{3}5s5p	^{2}G$_{7/2}$	435.1573	217.4	0.9	217		
31 907.74	4d^{3}5s5p	^{4}F$_{3/2}$	425.4693	725.4	11.0	725	820 (60)	Kröger (2007)[a]
32 087.58	4d^{4}5p	^{2}G$_{7/2}$	439.2692*	319.3	3.1	319	316 (2)	Başar et al. (2008)[a]
32 139.78	4d^{3}5s5p	^{4}G$_{5/2}$	426.6020	394.3	2.4	394		
32 213.94	4d^{3}5s5p	^{4}I$_{9/2}$	436.8434	594.8	1.5	595		
32 333.18	4d^{3}5s5p	^{4}F$_{7/2}$	429.2480	451.3	4.4	451		
32 382.24	4d^{3}5s5p	^{4}I$_{11/2}$	468.5133*	367.0	50‡	367		
32 451.99	4d^{2}5s^{2}5p	^{4}G$_{7/2}$	427.0691	421.6	3.0	422		
32 605.39	4d^{4}5p	^{2}G$_{9/2}$	432.6320	270.5	2.6			
			335.4743*	270.1	20.8	270.5 (1)	264.7 (4.0)	Singh et al. (1992)[a]
32 654.48	4d^{3}5s5p	^{4}F$_{3/2}$	430.6283*	321.0	11.1	321		
32 672.39	4d^{3}5s5p	^{4}I$_{13/2}$	466.6251*	530.7	30‡	531		
32 899.08	4d^{3}5s5p	^{4}F$_{7/2}$	441.1526	218.4	12.1	218		
33 116.36	4d^{3}5s5p	^{4}I$_{15/2}$	463.0115	627.1	20‡	627		
33 136.30	4d^{3}5s5p	^{4}F$_{9/2}$	422.9154	264.1	2.6	264		
34 004.08	4d^{4}5p	^{2}I$_{11/2}$	456.4530	294.1	1.7			
			405.1513*	291.4	11.2	294.1 (4)		
34 415.52	4d^{4}5p	^{4}I$_{9/2}$	427.7500*	330.6	50‡			
			425.5439	326.0	50‡	328 (2)		
34 654.79	4d^{3}5s5p	^{4}G$_{5/2}$	446.9714	198.6	2.8	199		
34 752.70	4d^{4}5p	^{2}D$_{3/2}$	405.9498	406.7	5.7	407		
34 838.33	4d^{4}5p	^{4}I$_{11/2}$	420.1519	281.5	50‡	282		
35 156.94	4d^{3}5s5p	^{4}G$_{9/2}$	434.2818	510.0	3.1	510	632.5 (6.0)	Singh et al. (1992)[a]
35 344.86	4d^{4}5p	^{4}I$_{11/2}$	411.3941*	379.8	50‡	380		
35 731.34	4d^{4}5p	^{4}I$_{15/2}$	412.9931	298.8	20‡	299		
36 717.11	4d^{3}5s5p	^{2}G$_{9/2}$	389.4039	306.3	20‡	306		

Notes. Level energies according to Humphreys & Meggers (1945); configurations and terms according to Kröger et al. (2007). The wavelength in air λ_{air} given in the fourth column specifies the line, that was used to determine the hyperfine constant A_{fit}; A_{fit} is the average result from eight measurements; ΔA_{fit} is the corresponding standard deviation. If more than one line was available for a level to determine A_{fit}, the weighted mean value A_{mean} is calculated, using ΔA_{fit} as weight. In column A_{mean} the standard deviation, that resulted from the weighted mean value calculation is given as error. If known, reference values A_{ref} from the literature are listed together with the indication of the method used. If more than one reference value has been published for a given level, only the most precise one is given.
[(a)] Optogalvanic spectroscopy; [(b)] saturation absorption spectroscopy; [(c)] laser induced fluorescence spectroscopy; [(d)] laser radio-frequency double resonance.
[(*)] FWHM and ratio between Gaussian and Lorentzian FWHM fixed during the fit; [(†)] error in sign in Başar et al. (2008); [(‡)] ΔA_{fit} is set equal to the uncertainty of the A_l-constant of the lower level.

in the spectra of metal-poor stars is crucial for determining if there indeed exist two different r-processes. Unfortunately, to date the niobium abundance was calculated only in the atmospheres of a few stars using a couple of identified lines in high resolution absorption spectra (Honda et al. 2006; Ivans et al. 2005; Yushchenko et al. 2004). Future studies of abundance patterns of neutron capture elements including niobium are encouraged to create a statistically significant sample of metal poor stars. The recent measurements of transition probabilities and hyperfine splittings reported for some elements should be incorporated.

6. Conclusion

We used high-resolution FT spectroscopy to obtain new and improved hyperfine structure data for neutral atomic Nb. Up to now, for atomic Nb the hyperfine structure constants A of 68 levels of odd parity have been published, determined by different experimental methods. With our investigations we extended the data for the odd parity levels by an additional 57 levels. That nearly doubles the data that can be used for a detailed and accurate interpretation of high-resolution stellar spectra including nuclear hyperfine structure effects.

Table 4. Results of the linear fits of the measured full width at half maximum (FWHM).

	Slope(MHz/cm^{-1})	Intercept(MHz)
Voigt	0.081 (1)	62 (18)
Gauss	0.070 (2)	40 (40)
Lorentz	0.019 (2)	40 (50)

Acknowledgements. I. K. Öztürk thanks the research fund of the Istanbul University project number 3307 and UDP-700/08032007. A. Er thanks the research fund of the Istanbul University project number 3164. We would like to

thank Florian Gahbauer for useful discussions and to acknowledge support from the Latvian Science Council Grant No. LZP 09.1196.

References

Başar, G., Başar, G., Bayram, B., & Kröger, S. 2008, Phys. Scr., 78, 015303
Booth, A. J., & Blackwell, D. E. 1983, MNRAS, 204, 777
Bouzed, A., Kröger, S., Zimmermann, D., Kronfeldt, H.-D., & Guthöhrlein, G. 2003, Eur. Phys. J. D, 23, 57
Burbidge, E. M., Burbidge, G. R., Fowler, W. A., & Hoyle, F. 1957, Rev. Mod. Phys., 29, 547
Büttgenbach, S., Dicke, R., Gebauer, H., Herschel, M., & Meisel, G. 1975, Z. Phys. D, 275, 193
Cowan, R. D. 1981, The theory of atomic structure and spectra (Berkeley, Los Angeles, London: University of California Press)
Fraenkel, L., Bengtsson, C., Hanstorp, D., Nyberg, A., & Persson, J. 1988, Z. Phys. D, 8, 171
Grevesse, N., Asplund, M., & Sauval, A. J. 2007, Space Sci. Rev., 130, 105
Guthöhrlein, G. 2004, university of Bundeswehr Hamburg, unpublished
Hannaford, P., Lowe, R. M., Biemont, E., & Grevesse, N. 1985, A&A, 143, 447
Honda, S., Aoki, W., Ishimaru, Y., Wanajo, S., & Ryan, S. G. 2006, ApJ, 643, 1180
Humphreys, C. J., & Meggers, W. F. 1945, J. Research Nat. Bur. Stand, 34, 478, 585
Ivans, I. I., Sneden, C., Gallino, R., Cowan, J. J., & Preston, G. W. 2005, ApJ, 627, L145
Kröger, S. 2007, Eur. Phys. J. D, 41, 55
Kröger, S., & Bouzed, A. 2003, Eur. Phys. J. D, 23, 63
Kröger, S., Scharf, O., & Guthöhrlein, G. 2004, Europhys. Lett., 66, 344
Kröger, S., Öztürk, I. K., Acar, F. G., et al. 2007, Eur. Phys. J. D, 41, 61
Kwiatkowski, M., Zimmermann, P., Biemont, E., & Grevesse, N. 1982, A&A, 112, 337
Lederer, C. M., & Shirley, V. S. 1978, Table of isotopes, 7th edn. (New York: Wiley)
Messnarz, D., & Guthöhrlein, G. H. 2000, Eur. Phys. J. D, 12, 269
Nilsson, H., & Ivarsson, S. 2008, A&A, 492, 609
Singh, R., & Rao, G. N. 1989, Phys. Scr., 40, 170
Singh, R., Thareja, R. K., & Rao, G. N. 1992, J. Opt. Soc. Am. B, 9, 493
Sneden, C., Cowan, J. J., & Gallino, R. 2008, Annu. Rev. Astro. Astrophys., 46, 241
Yushchenko, A. V., Gopka, V. F., Kim, C., et al. 2004, A&A, 413, 1105

Appendix A: Nb I lines of special interest for stellar spectroscopy

Figures A.1–A.29 show the Fourier transform spectra for lines of special interest for stellar spectroscopy. The hyperfine components are assigned by the difference ΔF of the total angular momentum of the upper and lower hyperfine levels. As summary, these lines are listed in Table A.1 (which is an extract from Table 1).

Table A.1. Nb I lines of special interest for stellar spectroscopy.

			Lower level		Upper level			
λ_{air}(nm)	$\tilde{\nu}$(cm^{-1})	Int.	E_l(cm^{-1})	J	E_u(cm^{-1})	J	$\tilde{\nu}_{fit}$(cm^{-1})	$\Delta\tilde{\nu}$(cm^{-1})
757.457	13 198.44	500	11 344.70	5/2	24 543.13	5/2	13 198.41	0.02
737.251	13 560.17	500	11 344.70	5/2	24 904.86	7/2	13 560.16	0.00
704.681	14 186.92	300	9 497.52	7/2	23 684.44	5/2	14 186.87	0.05
667.734	14 971.90	200	9043.14	5/2	24 015.11	7/2	14 972.02	–0.05
666.084	15 008.98	300	9497.52	7/2	24 506.53	9/2	15 008.98	0.03
590.059	16 942.77	200	9497.52	7/2	26 440.33	9/2	16 942.77	0.04
534.4160	18 706.83	200	2805.36	9/2	21 512.18	7/2	18 706.81	0.01
467.2097	21 397.69	200	2805.36	9/2	24 203.05	11/2	21 397.68	0.01
460.6760	21 701.17	200	2805.36	9/2	24 506.53	9/2	21 701.17	0.00
457.3077	21 861.01	200	2154.11	7/2	24 015.11	7/2	21 860.99	0.01
454.6820	21 987.25	120	1586.90	5/7	23 574.14	5/2	21 987.24	0.00
452.3409	22 101.04	200	1142.79	3/2	23 243.87	3/2	22 101.04	0.04
416.8122	23 984.88	250	0.00	1/2	23 984.87	1/2	23 984.85	0.02
416.4661	24 004.81	300	391.99	5/2	24 396.80	5/2	24 004.80	0.01
416.3658	24 010.60	250	154.19	3/2	24 164.79	3/2	24 010.59	0.01
415.2575	24 074.68	500	695.25	7/2	24 769.91	7/2	24 074.65	0.01
413.9702	24 149.54	400	1050.26	9/2	25 199.81	9/2	24 149.52	0.03
413.7090	24 164.79	200	0.00	1/2	24 164.79	3/2	24 164.77	0.02
412.3812	24 242.59	400	154.19	3/2	24 396.80	5/2	24 242.60	0.01
410.0918	24 377.93	600	391.99	5/2	24 769.91	7/2	24 377.91	0.01
407.9726	24 504.56	1000	695.25	7/2	25 199.81	9/2	24 504.55	0.01
405.8933	24 630.08	2000	1050.26	9/2	25 680.36	11/2	24 630.09	0.01
374.2393	26 713.31	200	0.00	1/2	26 713.32	3/2	26 713.31	0.01
373.9800	26 731.83	300	695.25	7/2	27 427.07	7/2	26 731.85	–0.03
372.6235	26 829.14	250	154.19	3/2	26 983.34	5/2	26 829.15	0.00
371.3018	26 924.64	300	1050.26	9/2	27 974.87	9/2	26 924.65	–0.04
358.0277	27 922.86	400	1050.26	9/2	28 973.12	7/2	27 922.87	–0.01
357.5850	27 957.43	200	695.25	7/2	28 652.66	5/2	27 957.43	–0.02
334.1982	29 913.79	200	1142.79	3/2	31 056.60	5/2	29 913.84	–0.03

Notes. For more details see Table 1.

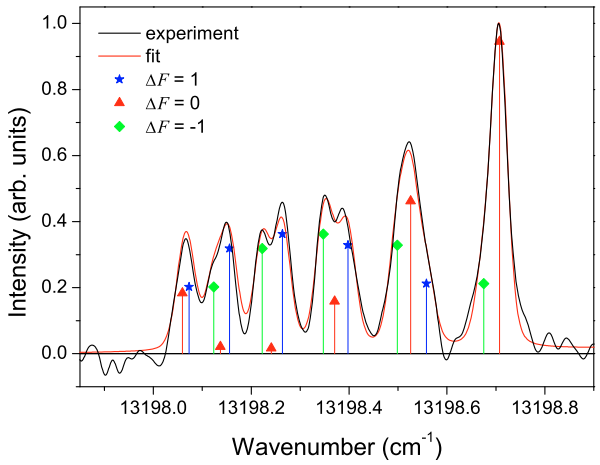

Fig. A.1. $\lambda_{\rm air}$ = 757.457 nm; $\tilde{\nu}$ = 13 198.44 cm^{-1}; transition 24 543.13 cm^{-1} (J = 5/2) ⟶ 11 344.70 cm^{-1} (J = 5/2).

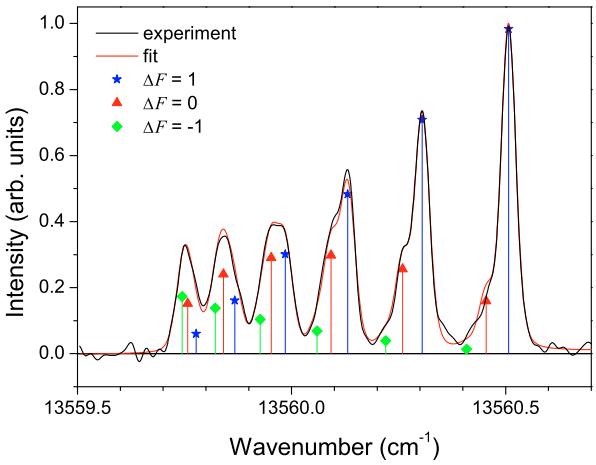

Fig. A.2. $\lambda_{\rm air}$ = 737.251 nm; $\tilde{\nu}$ = 13 560.17 cm^{-1}; transition 24 904.86 cm^{-1} (J = 7/2) ⟶ 11 344.70 cm^{-1} (J = 5/2).

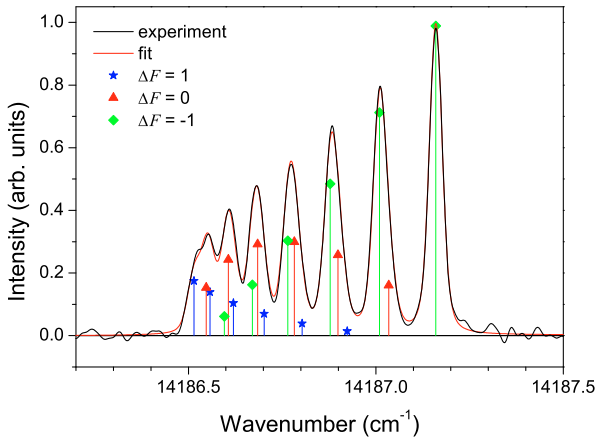

Fig. A.3. $\lambda_{\rm air}$ = 704.681 nm; $\tilde{\nu}$ = 14 186.92 cm^{-1}; transition 23 684.44 cm^{-1} (J = 5/2) ⟶ 9497.52 cm^{-1} (J = 7/2).

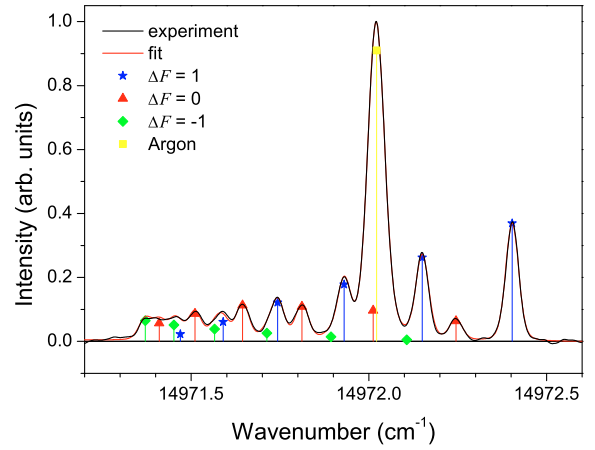

Fig. A.4. $\lambda_{\rm air}$ = 667.734 nm; $\tilde{\nu}$ = 14 971.90 cm^{-1}; transition 24 015.11 cm^{-1} (J = 7/2) ⟶ 9043.14 cm^{-1} (J = 5/2).

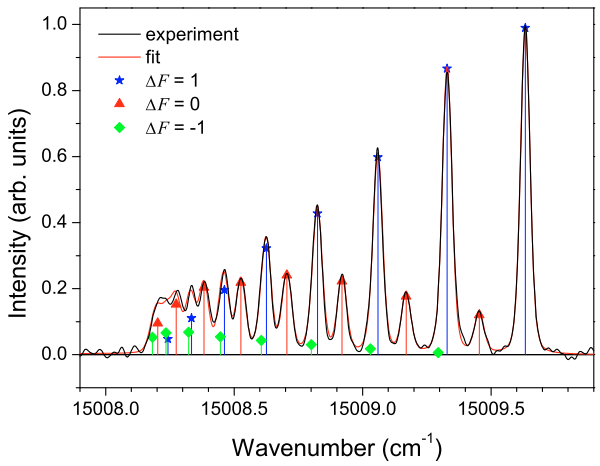

Fig. A.5. $\lambda_{\rm air}$ = 666.084 nm; $\tilde{\nu}$ = 15 008.98 cm^{-1}; transition 24 506.53 cm^{-1} (J = 9/2) ⟶ 9497.52 cm^{-1} (J = 7/2).

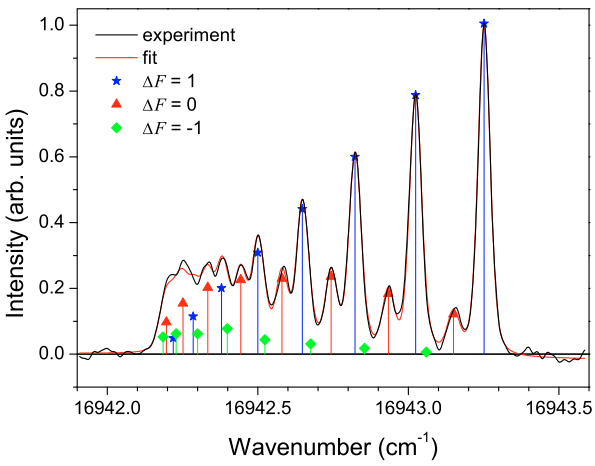

Fig. A.6. $\lambda_{\rm air}$ = 590.059 nm; $\tilde{\nu}$ = 16 942.77 cm^{-1}; transition 26 440.33 cm^{-1} (J = 9/2) ⟶ 9497.52 cm^{-1} (J = 7/2).

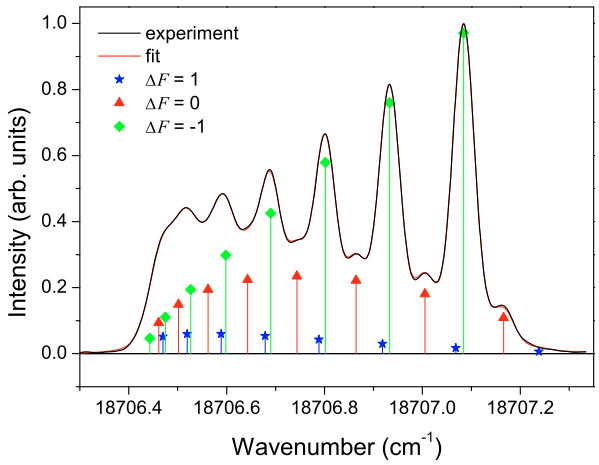

Fig. A.7. $\lambda_{\rm air}$ = 534.4160 nm; $\tilde{\nu}$ = 18 706.83 cm^{-1}; transition 21 512.18 cm^{-1} (J = 7/2) ⟶ 2805.36 cm^{-1} (J = 9/2).

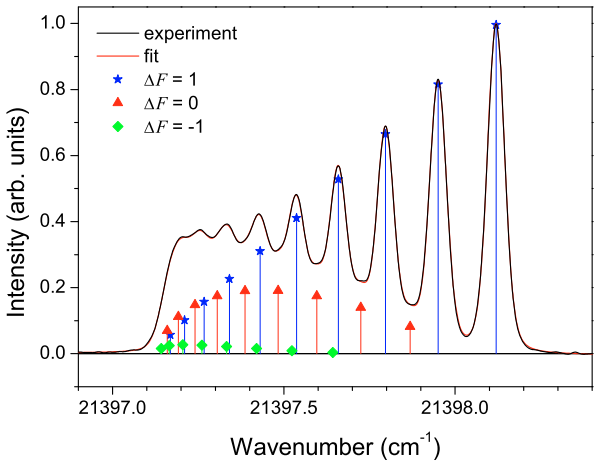

Fig. A.8. $\lambda_{\rm air}$ = 467.2097 nm; $\tilde{\nu}$ = 21 397.69 cm^{-1}; transition 24 203.05 cm^{-1} (J = 11/2) ⟶ 2805.36 cm^{-1} (J = 9/2).

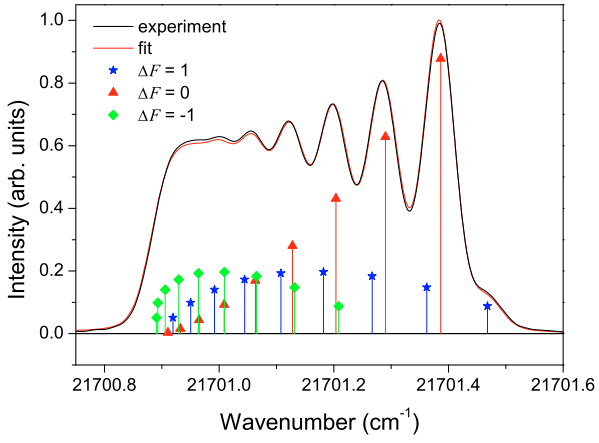

Fig. A.9. $\lambda_{\rm air}$ = 460.6760 nm; $\tilde{\nu}$ = 21 701.17 cm^{-1}; transition 24 506.53 cm^{-1} (J = 9/2) ⟶ 2805.36 cm^{-1} (J = 9/2).

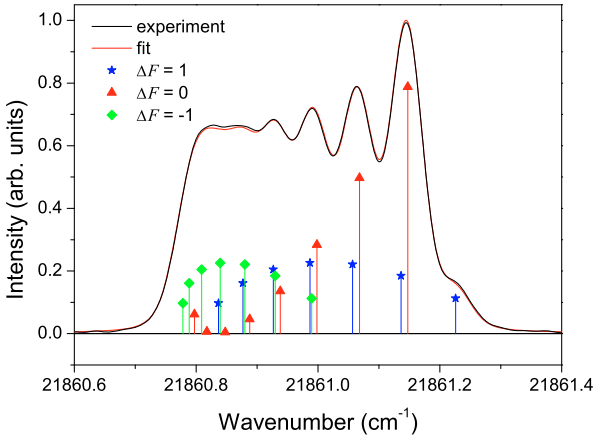

Fig. A.10. $\lambda_{\rm air}$ = 457.3077 nm; $\tilde{\nu}$ = 21 861.01 cm^{-1}; transition 24 015.11 cm^{-1} (J = 7/2) ⟶ 2154.11 cm^{-1} (J = 7/2).

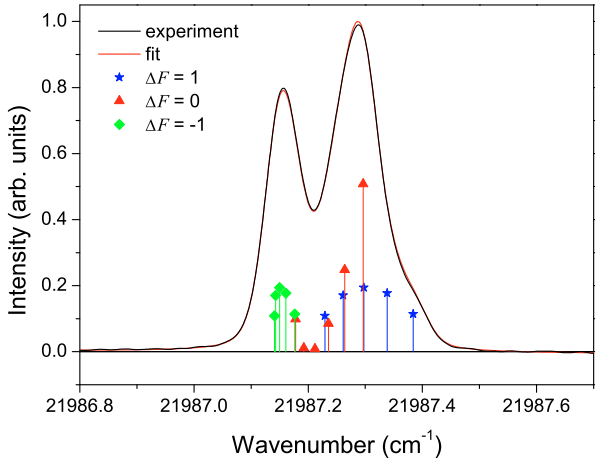

Fig. A.11. $\lambda_{\rm air}$ = 454.6820 nm; $\tilde{\nu}$ = 21 987.25 cm^{-1}; transition 23 574.14 cm^{-1} (J = 5/2) ⟶ 1586.90 cm^{-1} (J = 5/2).

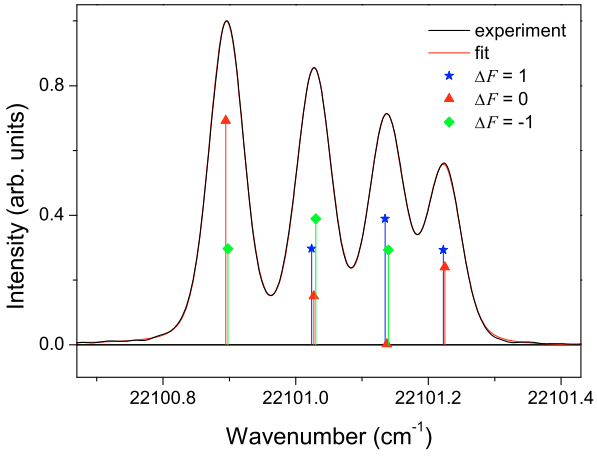

Fig. A.12. $\lambda_{\rm air}$ = 452.3409 nm; $\tilde{\nu}$ = 22 101.04 cm^{-1}; transition 23 243.87 cm^{-1} (J = 3/2) ⟶ 1142.79 cm^{-1} (J = 3/2).

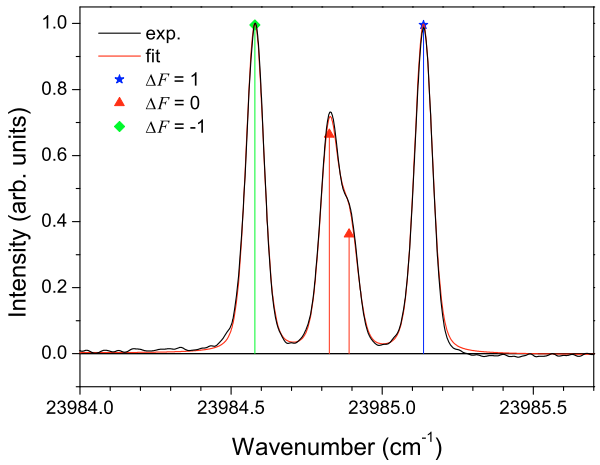

Fig. A.13. $\lambda_{\rm air}$ = 416.8122 nm; $\tilde{\nu}$ = 23 984.88 cm^{-1}; transition 23 984.87 cm^{-1} (J = 1/2) ⟶ 0.00 cm^{-1} (J = 1/2).

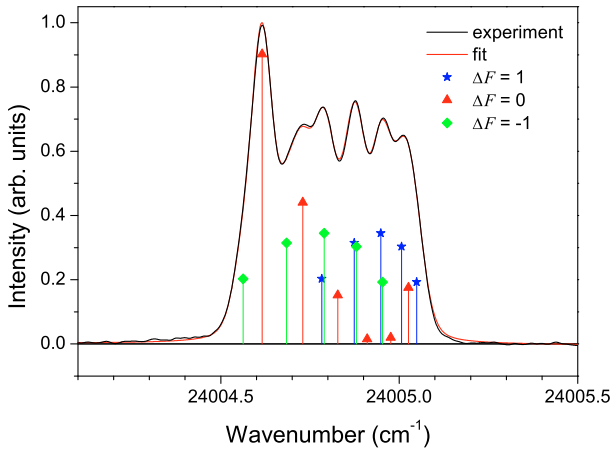

Fig. A.14. $\lambda_{\rm air}$ = 416.4661 nm; $\tilde{\nu}$ = 24 004.81 cm^{-1}; transition 24 396.80 cm^{-1} (J = 5/2) ⟶ 391.99 cm^{-1} (J = 5/2).

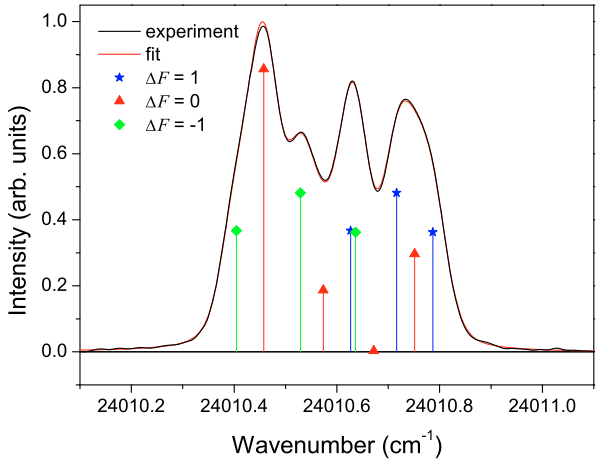

Fig. A.15. $\lambda_{\rm air}$ = 416.3658 nm; $\tilde{\nu}$ = 24 010.60 cm^{-1}; transition 24 164.79 cm^{-1} (J = 3/2) ⟶ 154.19 cm^{-1} (J = 3/2).

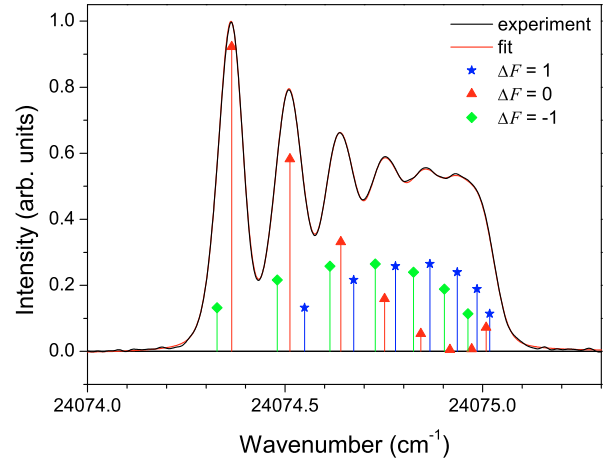

Fig. A.16. $\lambda_{\rm air}$ = 415.2575 nm; $\tilde{\nu}$ = 24 074.68 cm^{-1}; transition 24 769.91 cm^{-1} (J = 7/2) ⟶ 695.25 cm^{-1} (J = 7/2).

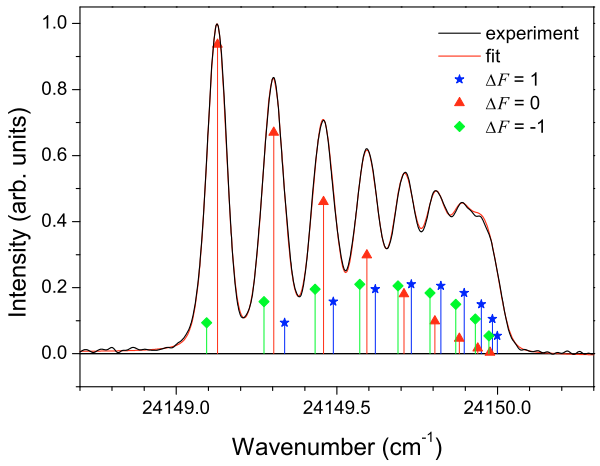

Fig. A.17. $\lambda_{\rm air}$ = 413.9702 nm; $\tilde{\nu}$ = 24 149.54 cm^{-1}; transition 25 199.81 cm^{-1} (J = 9/2) ⟶ 1050.26 cm^{-1} (J = 9/2).

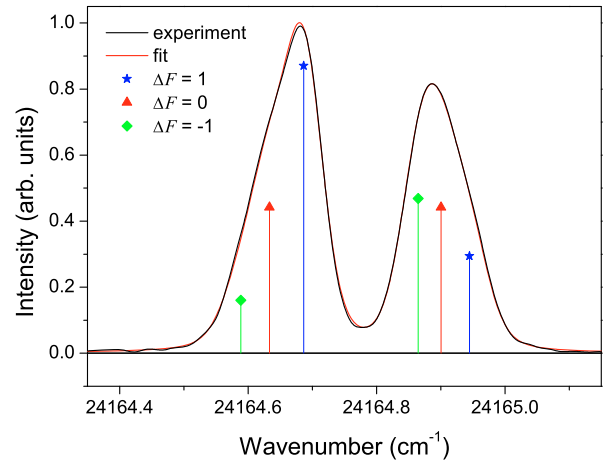

Fig. A.18. $\lambda_{\rm air}$ = 413.7090 nm; $\tilde{\nu}$ = 24 164.79 cm^{-1}; transition 24 164.79 cm^{-1} (J = 3/2) ⟶ 0.00 cm^{-1} (J = 1/2).

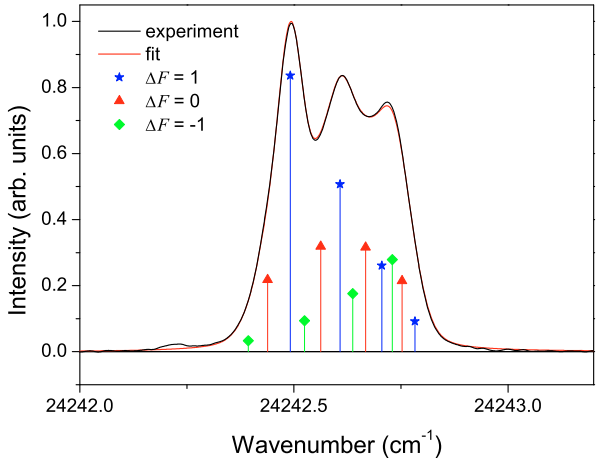

Fig. A.19. $\lambda_{\rm air}$ = 412.3812 nm; $\tilde{\nu}$ = 24 242.59 cm^{-1}; transition 24 396.80 cm^{-1} (J = 5/2) ⟶ 154.19 cm^{-1} (J = 3/2).

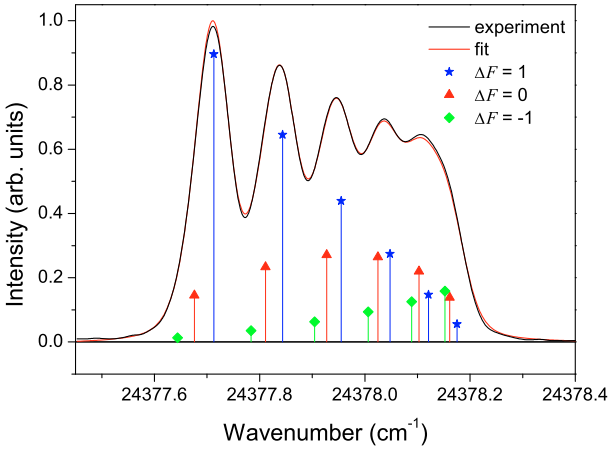

Fig. A.20. $\lambda_{\rm air}$ = 410.0918 nm; $\tilde{\nu}$ = 24 377.93 cm^{-1}; transition 24 769.91 cm^{-1} (J = 7/2) ⟶ 391.99 cm^{-1} (J = 5/2).

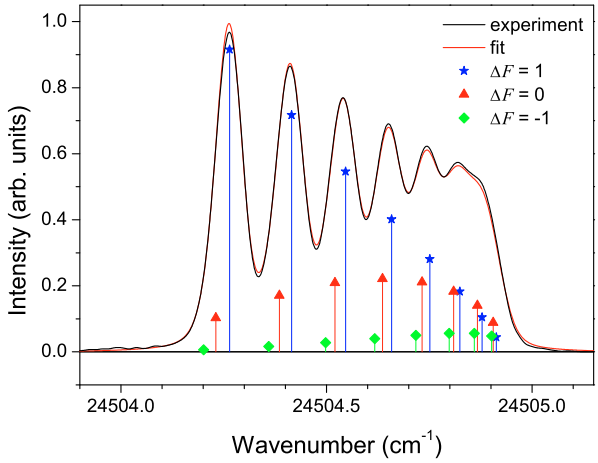

Fig. A.21. $\lambda_{\rm air}$ = 407.9726 nm; $\tilde{\nu}$ = 24 504.56 cm^{-1}; transition 25 199.81 cm^{-1} (J = 9/2) ⟶ 695.25 cm^{-1} (J = 7/2).

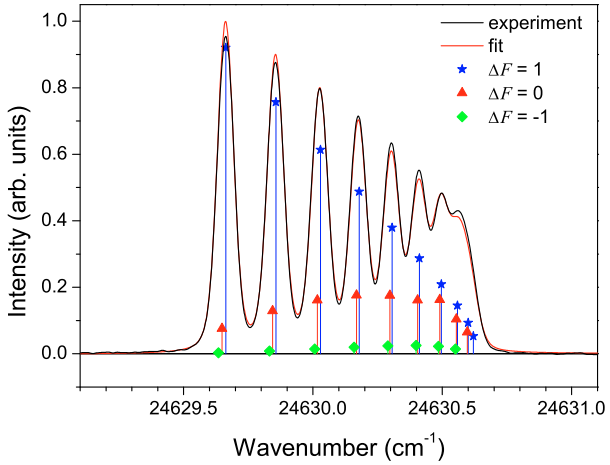

Fig. A.22. $\lambda_{\rm air}$ = 405.8933 nm; $\tilde{\nu}$ = 24 630.08 cm^{-1}; transition 25 680.36 cm^{-1} (J = 11/2) ⟶ 1050.26 cm^{-1} (J = 9/2).

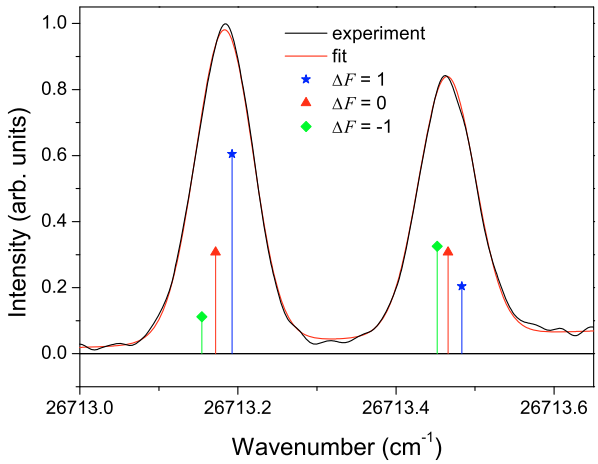

Fig. A.23. $\lambda_{\rm air}$ = 374.2393 nm; $\tilde{\nu}$ = 26 713.31 cm^{-1}; transition 26 713.32 cm^{-1} (J = 3/2) ⟶ 0.00 cm^{-1} (J = 1/2).

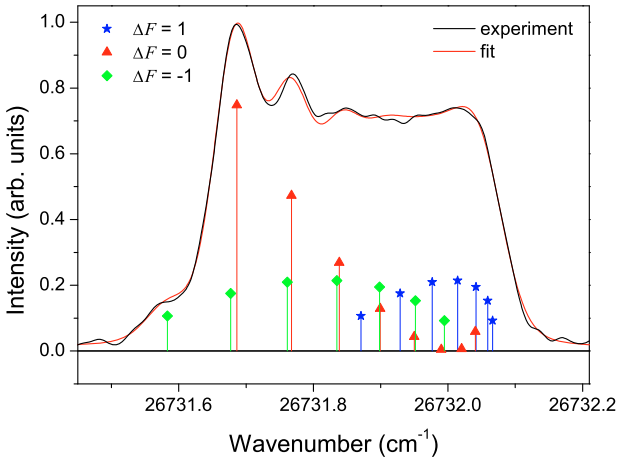

Fig. A.24. $\lambda_{\rm air}$ = 373.9800 nm; $\tilde{\nu}$ = 26 731.83 cm^{-1}; transition 27 427.07 cm^{-1} (J = 7/2) ⟶ 695.25 cm^{-1} (J = 7/2).

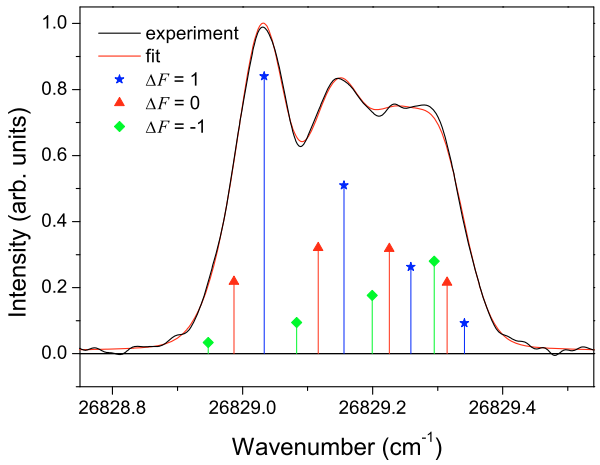

Fig. A.25. $\lambda_{\rm air}$ = 372.6235 nm; $\tilde{\nu}$ = 26 829.14 cm^{-1}; transition 26 983.34 cm^{-1} (J = 5/2) $\longrightarrow$ 154.19 cm^{-1} (J = 3/2).

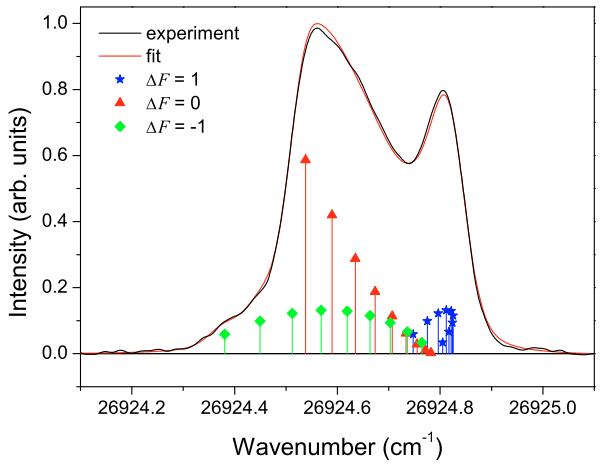

Fig. A.26. $\lambda_{\rm air}$ = 371.3018 nm; $\tilde{\nu}$ = 26 924.64 cm^{-1}; transition 27 974.87 cm^{-1} (J = 9/2) $\longrightarrow$ 1050.26 cm^{-1} (J = 9/2).

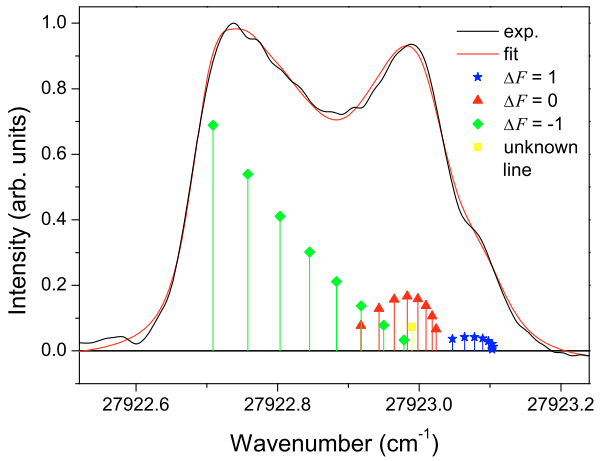

Fig. A.27. $\lambda_{\rm air}$ = 358.0277 nm; $\tilde{\nu}$ = 27 922.86 cm^{-1}; transition 28 973.12 cm^{-1} (J = 7/2) $\longrightarrow$ 1050.26 cm^{-1} (J = 9/2).

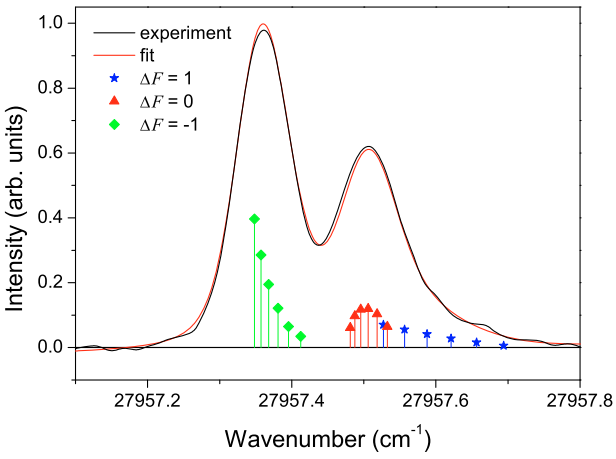

Fig. A.28. $\lambda_{\rm air}$ = 357.5850 nm; $\tilde{\nu}$ = 27 957.43 cm^{-1}; transition 28 652.66 cm^{-1} (J = 5/2) $\longrightarrow$ 695.25 cm^{-1} (J = 7/2).

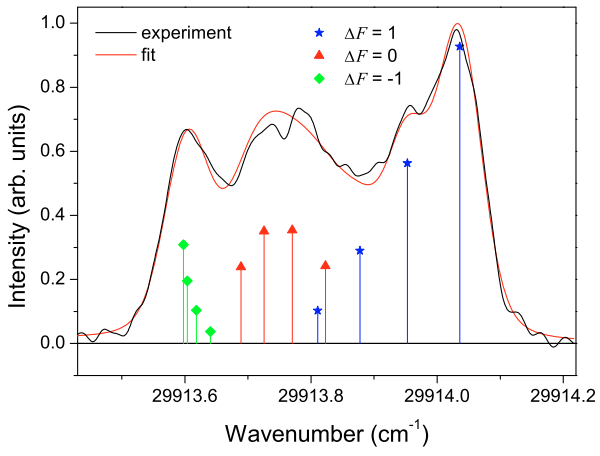

Fig. A.29. $\lambda_{\rm air}$ = 334.1982 nm; $\tilde{\nu}$ = 29 913.79 cm^{-1}; transition 31 056.60 cm^{-1} (J = 5/2) $\longrightarrow$ 1142.79 cm^{-1} (J = 3/2).